Induced CD8α Identifies Human NK cells with Enhanced Proliferative Fitness and Modulates NK cell Activation

Celia C. Cubitt,[1] Pamela Wong,[1] Hannah K. Dorando,[2] Jennifer A. Foltz,[1] Jennifer Tran,[1] Lynne Marsala,[1] Nancy D. Marin,[1] Mark Foster,[1] Timothy Schappe,[1] Hijab Fatima,[3] Michelle Becker-Hapak,[1] Alice Y. Zhou,[1] Kimberly Hwang,[1] Miriam T. Jacobs,[1] David A. Russler-Germain,[1] Emily M. Mace,[3] Melissa M. Berrien-Elliott,[1] Jacqueline E. Payton,[2] Todd A. Fehniger[1]

[1]Division of Oncology, Siteman Cancer Center, Washington University School of Medicine, St. Louis, MO, USA

[2]Department of Pathology and Immunology, Washington University School of Medicine, St. Louis, MO, USA

[3]Division of Allergy, Immunology and Rheumatology, Department of Pediatrics, Columbia University Vagelos College of Physicians and Surgeons, New York, NY, USA

[§]Correspondence: Todd A. Fehniger, MD/PhD
Washington University School of Medicine, 425 South Euclid Avenue, Campus Box 8007, St. Louis, MO 63110, Office: (314) 362-5654, Fax: (314) 362-9333, tfehnige@wustl.edu

Running title: CD8α identifies IL-15-induced biology and modulates activation in human NK cells

Abstract word count: 199 (max 200)
Figure and table count: 8
Supplemental Figure and table count: 12
Total word count = 11938 (max 12000)

Keywords: NK cells, CD8α, IL-15, proliferation, metabolism, anti-tumor activity, NK cell activating receptors

Abstract

The surface receptor CD8α is present on 20-80% of human (but not mouse) NK cells, yet its function on NK cells remains poorly understood. CD8α expression on donor NK cells was associated with a lack of therapeutic responses for leukemia patients in prior studies, thus we hypothesized that CD8α may impact critical NK cell functions. Here, we discovered that CD8α- NK cells had improved control of leukemia in xenograft models, compared to CD8α+ NK cells, likely due to an enhanced capacity for proliferation. Unexpectedly, CD8α expression was induced on approximately 30% of previously CD8α- NK cells following IL-15 stimulation. These 'induced' CD8α+ ('iCD8α+') NK cells had the greatest proliferation, responses to IL-15 signaling, and metabolic activity, compared to those that sustained existing CD8α expression ('sustained CD8α+) or those that remained CD8α- ('persistent CD8α-'). These iCD8α+ cells originated from an IL-15Rβ high NK cell population, with CD8α expression dependent on the transcription factor RUNX3. Moreover, *CD8A* CRISPR/Cas9 deletion resulted in enhanced responses through the activating receptor NKp30, possibly by modulating KIR inhibitory function. Thus, CD8α status identifies human NK cell capacity for IL-15-induced proliferation and metabolism in a time-dependent fashion and exhibits a suppressive effect on NK cell activating receptors.

Highlights

- CD8α- NK cells mediate superior in vivo tumor control
- CD8α- NK cells exhibit enhanced capacity for proliferation
- Induced CD8α identifies human NK cells with enhanced IL-15 signaling, proliferation, and metabolism
- Deletion of *CD8A* in human NK cells results in enhanced responses via activating NK cell receptors

Introduction

NK cells are innate lymphoid cells that protect the host from infection and malignant transformation through direct cytotoxicity and communication via cytokine and chemokine production (1–3). Human NK cells are characterized as two distinct subsets in human peripheral blood, the immature and highly proliferative $CD56^{bright}$ subset, and the mature, less proliferative and more cytotoxic $CD56^{dim}$ subset (1, 4). NK cell function is tightly regulated by a balance of germ-line DNA-encoded activating, inhibitory, and cytokine receptors (5, 6). The primary inhibitory receptors in human NK cells that promote self-tolerance include the killer cell immunoglobulin (Ig)-like receptors (KIRs) that bind to MHC class I, and the CD94-NKG2A receptor that recognizes the non-polymorphic human leukocyte antigen-E (HLA-E) (7–9). NK cells also express multiple activating receptors that trigger effector functions when engaged, including the natural cytotoxicity receptors (NCRs) NKp30 and NKp46, the C-type lectin NKG2D, and other co-receptors such as CD16, CD2, and 2B4 (4, 5, 10). While signaling through these receptors has been described to occur by associating with a variety of shared (CD16 and NKp30: CD3z / FcRγ) and distinct (NKG2D: DAP10; 2B4: SAP and Fyn; CD2:p56lck) signaling adaptors, additional mechanisms that modulate these signals are not clearly understood (10–13).

NK cells are particularly dependent on IL-15 signaling for their proliferation and survival (14–16). The IL-15 receptor is composed of three subunits: IL-2/15Rα (CD25), IL-15Rβ (CD122), and the shared common γ (CD132) chain. IL-15 receptor signals via three distinct pathways via JAK1,3/STAT5 (STAT5), Ras/Raf/Mek/Erk (MAPK), and PI3K/Akt/mTOR (AKT-mTOR), which drive transcriptional and metabolic programs that control NK homeostasis and proliferation (14, 17, 18). In particular, mTOR activation leads to translation initiation (by phosphorylating ribosomal protein 6 [S6]) and modulates metabolism via the upregulation of nutrient receptors and proteins involved in glycolysis and lipid synthesis (19, 20). Supporting this, studies in murine NK cells have established that glucose metabolism is essential for IL-15 driven proliferation (21, 22).

The biology of the coreceptor CD8α on human NK cells is not well understood, and mouse NK cells do not express CD8α (23). On average, 40% (range 15-88%) of human NK cells express the homodimeric CD8$\alpha\alpha$ receptor, and a small proportion (1-2%) express the CD8$\alpha\beta$ heterodimer (24, 25). While CD8$\alpha\beta$ has been extensively characterized on T cells as a co-receptor for TCR, CD8$\alpha\alpha$ is expressed on other immune cells,

including intraepithelial lymphocytes, human monocytes, and murine dendritic cells (26–28). CD8αα contains an extracellular region that can bind to the conserved α3 region of HLA class I and most non-classical HLA [except human HLA-E, due to α3 domain polymorphisms (29, 30)], a transmembrane domain, and a cytoplasmic tail that associates with the Src tyrosine kinase Lck (26). There are limited and conflicting data on the function of CD8α on the biology of human NK cells. Previous studies have described that CD8α positive (CD8α+) NK cells are more cytotoxic and mediate leukemia cell killing in patients who received autologous hematopoietic cell transplants (HCT), although this study compared CD8α+/- NK cells without accounting for the higher expression of CD8α on the more mature and cytotoxic $CD56^{dim}$ subset (31). In patients with untreated chronic HIV infections, higher frequencies of CD8α+ NK cells were correlated with slower disease progression, while a CD8+ NK transcriptomic signature was associated with reduced relapse risk in patients with relapsing remitting multiple sclerosis (32, 33). Additional conflicting effects have also been reported, with CD8α protecting NK cells from activation-induced apoptosis in one study, and CD8α engagement with soluble HLA class I triggering apoptosis in another (34, 35). A more recent study proposed that CD8α could facilitate NK cell licensing by binding to HLA class I and enhancing KIR binding (36).

Allogenic NK cellular immunotherapies have been investigated for treating cancer in multiple clinical trials (37, 38). Our previous work has identified that NK cells briefly stimulated with IL-12, IL-15, and IL-18 become long-lived, memory-like (ML) NK cells with the ability to respond robustly upon restimulation with cytokines and activating receptors, including CD16 engagement with tumor-targeting monoclonal antibody (24, 39–41). Correlative immunology from a study using ML NK cells as a cellular therapy for relapsed / refractory acute myeloid leukemia (AML) identified a negative association between CD8α expression on donor ML NK cells and treatment outcome, such that expression of CD8α was higher on donor NK cells in patients experiencing treatment failure (24). Further work identified that CD8α negative (CD8α-) ML NK cells had enhanced proliferation in patients, and sorted CD8α- ML NK cells had a proliferative advantage in vitro. However, the biology and mechanisms associated with this finding, and how they extend to conventional (c) NK cells, remain unclear.

Here, we examined the biology of CD8α on human cNK cells and discovered an unexpected time-dependent association with IL-15 signaling, metabolism, and proliferation. Further, we define a functional role for CD8α in regulating human NK cell activation.

Results

CD8α- NK cells have enhanced tumor control *in vivo*

Our prior study identified a negative association between CD8α expression on donor ML NK cells and treatment outcome, and that ML CD8α+ NK cells had impaired proliferation in vitro (24). We examined the expression of CD8α on human cNK cells, and found that CD8α was expressed by both $CD56^{bright}$ and $CD56^{dim}$ NK cell populations, and that the percent of CD8α+ NK cells was variable (**Figure 1, A-C**). Notably, a greater proportion of $CD56^{dim}$ NK cells express CD8α compared to $CD56^{bright}$ NK cells at baseline. Consistent with prior findings, CD8αα was the dominant form expressed, while a small fraction (<5%) expressed CD8αβ heterodimers (**Supplemental Figure 1A**) (24). In agreement with previous literature (23), we also confirmed that CD8α was not expressed on murine NK cells (**Supplemental Figure 1B**), precluding studies using murine models. We next sought to determine whether CD8α expression on the mature and cytotoxic $CD56^{dim}$ population corresponded to differences in the ability to control tumors in vivo. We sorted CD8α+ or CD8α- $CD56^{dim}$ cNK cells, administered (i.v.) to groups of NOD-SCID-IL-$2R\gamma^{-/-}$ (NSG) mice, supported with recombinant human (rh)-IL-15 (i.p.), then challenged with K562-luciferase tumor cells and monitored tumor burden via bioluminescent imaging (BLI) (**Figure 1D**). We found that mice treated with sorted CD8α- NK cells had lower tumor burden compared to those that received CD8α+ NK cells, or no NK cells at all (**Figure 1, E and F)**. Notably, CD8α- and CD8α+ treated mice had similar tumor control initially (Days 1 and 4), and differences between the groups became more apparent at later time points (Days 7-15). Given that K562 cells lack HLA class I expression, we next sought to determine if CD8α- NK cells had enhanced responses against the HLA-expressing tumor lines Jeko-1 and HL60. Since NKs are inhibited through KIR interaction with self-HLA, we compared the functional responses of CD8α+ or CD8α- KIR3DL1, KIR2DL2/3, or KIR2DL1 single positive (NKG2A- $CD56^{dim}$) NK cells. We found that CD8α- KIR2DL2/3 and KIR2DL1 single positive NK cells had higher expression of IFNγ following stimulation with both Jeko-1 and HL60 cell lines, compared to those that were CD8α+. There was no difference within KIR3DL1 single

positive NK cells, suggesting this effect may depend on the particular KIR-HLA combination engaged (**Supplemental Figure 1C-E**). These data demonstrate that CD8α- NK cells have an enhanced capacity to control tumors in leukemia-xenografted mice and in vitro, compared to CD8α+ NK cells.

CD8α- NK cells have enhanced proliferation and survival in vitro and in vivo

Since the ability of adoptively transferred allogeneic NK cells to eliminate residual leukemic cells relies on their persistence and expansion in vivo (40, 42), we sought to identify any proliferative differences between CD8α+ or CD8α- NK cells. To determine the proliferative capacity of CD8α+ cNK cells, freshly isolated NK cells were labeled with cell-trace violet (CTV), sorted based on CD8α expression, and cultured in IL-15 in vitro for 9 days (**Figure 2A**). Sorted CD8α- NK cells exhibited significantly increased proliferation (**Figure 2, B and C, Supplemental Figure 2A**), compared to sorted CD8α+ NK cells in vitro. Since $CD56^{dim}$ NK cells have significantly higher expression of CD8α (**Figure 1C**) and are less proliferative than $CD56^{bright}$ NK cells (1, 4), we also evaluated proliferation using sorted $CD56^{dim}$ NK cells (**Supplemental Figure 2B**). Consistent with bulk NK cells, CD8α- $CD56^{dim}$ NK cells had significantly higher proliferation, compared to sorted CD8α+ $CD56^{dim}$ NK cells (**Figure 2D**). Since IL-15 also regulates NK cell survival in addition to proliferation, we utilized 7AAD and Annexin V staining to identify any differences in survival of these populations (14, 43, 44). Notably, CD8α- $CD56^{dim}$ NK cells had significantly increased survival after IL-15 culture in vitro, compared to CD8α+ $CD56^{dim}$ NK cells (**Figure 2E**). Based on these in vitro studies, we hypothesized that CD8α- $CD56^{dim}$ NK cells also have an enhanced proliferative capacity in vivo. Human cNK cells were labeled with CTV, $CD56^{dim}$ NK cells were sorted based on CD8α expression, and CD8α+ $CD56^{dim}$ or CD8α- $CD56^{dim}$ NK cells were injected i.v. into NSG mice (**Figure 2F**). NK cells were supported with rh-IL-15 and after 9 days, human NK cells were isolated from the blood, spleen, and liver from these mice. Sorted CD8α- $CD56^{dim}$ NK cells had robust proliferation within the liver (**Figure 2, G and H**), in addition to the blood and spleen (**Supplemental Figure 2, C and D**). Further, the absolute number of NK cells was significantly higher in the liver of mice that received CD8α- $CD56^{dim}$ NK cells (**Supplemental Figure 2E**). Thus, sorted CD8α- $CD56^{dim}$ NK cells underwent significantly increased proliferation and expansion in vitro and in vivo with IL-15 support, compared to sorted CD8α+ $CD56^{dim}$ NK cells.

CD8α does not mark a distinct, terminally differentiated population

Next, potential mechanisms responsible for the proliferative differences based on CD8α expression were investigated. Since CD8α was expressed on both CD56^{bright} and CD56^{dim} NK subsets, we reasoned that rather than marking a terminal differentiation event, CD8α may represent a distinct functional or activation state. This was first evaluated via bulk RNA sequencing of sorted CD8α+/- CD56^{bright} and CD56^{dim} NK cells, which revealed similar transcriptional profiles between the populations (**Figure 3, A and B, Supplemental Figure 3, A and B**). CD8A mRNA was significantly higher in CD8α+ NK cells, supporting that transcript abundance was responsible for CD8α protein differences. In addition, we analyzed single-cell RNA sequencing (scRNAseq) of primary human NK cells, and CD8α did not associate with or identify a unique subset, as defined by UMAP clustering (**Supplemental Figure 3, C and D**). These data suggest that CD8α does not mark a subset of NK cells with a distinct gene expression program. Consistent with this finding, mass cytometry phenotyping of CD56^{bright} and CD56^{dim} cNK cells identified minor differences in the frequency of activating receptors (**Supplemental Figure 3, E and F**). To determine if CD8α was associated with a particular maturation stage, CD8α expression was evaluated within an established progression of CD56^{dim} maturation, characterized by the loss of NKG2A expression and the acquisition of KIR (defined here as KIR3DL1+, KIR2DL1+, and KIR2DL2/3+) and CD57. CD8α expression was modestly increased on the terminally matured NKG2A- KIR+ CD57+ CD56^{dim} subset, compared to the immature NKG2A- KIR- CD57- population. Interestingly, CD8α expression was highest on KIR-positive CD56^{dim} and CD56^{bright} subsets, compared to KIR-negative subsets (**Figure 3, C and D).** NK cells acquire functional competence via education or licensing through KIR interactions with self-HLA (45). Since CD8α binds HLA on the conserved α3 domain, while KIR bind a polymorphic site on the α2 domain, we hypothesized that CD8α may be enriched on KIR-licensed versus unlicensed NK cells. To assess this, we identified NKG2A- KIR single positive licensed or unlicensed CD56^{dim} NK cells (46) and compared licensed to unlicensed KIR+ NK cells within donors (**Supplemental Figure 4A)** or across individual KIR single positive CD56^{dim} NK cells (**Supplemental Figure 4B**). This revealed no significant differences in CD8α expression based on self-KIR licensing status. Collectively, these data suggest that CD8α does not identify a distinct subset of NK cells defined transcriptionally, via maturation, or by licensing; however, CD8α expression is enriched on KIR+ NK cells.

IL-15 modulates CD8α expression on CD8α- NK cells via RUNX3

CD8α is variably expressed on freshly isolated NK cells, and the signals that control expression are not defined. To address this, we sorted CD8α+ and CD8α- $CD56^{dim}$ NK cells and evaluated CD8α expression after cytokine stimulation. We discovered that while sorted CD8α+ $CD56^{dim}$ NK cells maintained CD8α expression, a subset of sorted CD8α- $CD56^{dim}$ NK cells upregulated CD8α over time in culture (**Figure 4A**), and this effect was IL-15 dose-dependent (**Supplemental Figure 5A**). In contrast, while $CD56^{bright}$ NK cells have lower expression of CD8α on freshly isolated NK cells (**Figure 1C**), nearly all (80%) sorted CD8α- $CD56^{bright}$ NK cells became CD8α positive in culture with IL-15 (**Supplemental Figure 5B**). The small percentage of CD8αβ+ $CD56^{dim}$ NK cells remained constant throughout stimulation, indicating that IL-15 independently induces CD8α but not CD8β expression (**Supplemental Figure 5, C and D**). This led us to hypothesize that the timing of CD8α acquisition may be a determinant of cytokine-stimulation or proliferation status, and that induced CD8α expression was marking a population that was robustly responding to IL-15 signals. To address this, we sorted CD8α- and CD8α+ $CD56^{dim}$ NK cells, cultured them in vitro with IL-15 for at least 6 days, and gated on CD8α expression **(Figure 4, B and C**). This approach allowed us to isolate the expression of CD8α in time and assess the biological features of 'sustained' CD8α+ NK cells (sorted CD8α+ NK that sustained CD8α expression) versus induced CD8α+ ('iCD8α+', sorted CD8α- NK that acquired CD8α expression during culture) and persistent "CD8α-" (CD8α- NK cells that remained CD8α-). After 6 days, almost all sorted CD8α+ NK cells remained sustained CD8α+. However, approximately 30% of sorted CD8α- NK cells became iCD8α+, and the remainder were persistent CD8α- (**Figure 4C**). Unexpectedly, we discovered that NK cells with induced CD8α expression were the most proliferative, compared to those that remained CD8α- or those that sustained CD8α expression, and this effect was consistent both in vitro and in vivo within NSG mice (**Figure 4D**). To further characterize the factors that regulate CD8α expression, we examined the expression of RUNX3, a transcription factor that has predicted binding sites located within putative regulatory regions in the CD8A gene locus (47). We found that RUNX3 expression was higher in iCD8α+ NK cells, as compared to 'sustained' CD8α+ or 'persistent' CD8α- NK cells (**Figure 5A**). Further, we found that CRISPR/Cas9 gene editing of *RUNX3* and subsequent transfer into NSG mice to allow for robust proliferation (**Figure 5B, Supplemental Figure 5E)** resulted in decreased

expression of CD8α in sorted CD8α+ NK cells (**Figure 5C)** and abrogated upregulation of CD8α in sorted CD8α- NK cells (**Figure 5D**). To further interrogate whether RUNX3 regulates CD8α at the transcriptional level, we used CUT&TAG (48) to compare the abundance of H3K27ac, an epigenetic modification of histones in promoters, enhancers, and gene bodies that is correlated with active transcription, in control and *RUNX3* KO NK cells. Using log2 fold change (log2 FC) and matched paired t-test for RUNX3 deletion and control, we required $p<0.05$ and that at least three of four donors had a log2 FC $\geq$ absolute 0.5. We found that loss of RUNX3 led to a decrease in total H3K27ac signal within the *CD8A* locus with log2 FC -0.9 to -8.6 for three of four donors, with one donor having low H3K27ac abundance in both control and *RUNX3* KO conditions (**Figure 5E**). This analysis also identified 174 genes with lower H3K27ac signal and 23 genes with higher H3K27ac signal in *RUNX3* KO. Notably, deletion of RUNX3 led to a decrease in H3K27ac peaks near genes involved in NK cell function / activation (*GZMB, CSK, LAT, IRAK4, TGFBR1, KIR2DL4, KIR2DL3, TNFSF14, PLCB2, CCL5, S1PR5)*, translation initiation (*EIF2AK1, EIF2B2*), and nutrient transport (*SLC39A6, SLC1A5, SLC35A5, SLC50A1*), and an increase in H3K27ac peaks near genes related to NK cell development (*IKZF3*/*Aiolos*) and signaling (*CXC4, TSC1, VAV3*); no H3K27ac peaks were detected in the *CD8B* promoter or gene body (**Figure 5F, Supplemental Figure 5F)**. Taken together, these data demonstrate that IL-15 induces CD8α expression, recent CD8α upregulation marks highly proliferative cells, and RUNX3 regulates expression of *CD8A* and other genes related to NK cell proliferation and activation.

IL-15R density determines NK cell proliferation and upregulation of CD8α after IL-15 stimulation

There are three IL-15 receptor subunits: IL-15Rα, IL-2/15Rβ (CD122), and the shared common γ chain (γc, CD132) (14, 49). IL15Rα binds to IL-15 with high affinity and facilitates trans-presentation to the signaling components of the IL-15R on NK cells (IL-15Rβγc). While all mature NK cells are positive for IL-15Rβγc expression and begin to acquire and maintain CD122 (IL-2/15Rβ) as they progress to the $CD56^{bright}$ stage (50), the receptor components are expressed at varying densities on human NK cells (17, 51). We hypothesized that differential expression of these receptor components could be driving the enhanced proliferation in iCD8α+ NK cells. Notably, we found that iCD8α+ $CD56^{dim}$ NK cells had significantly higher expression of CD132 (γ_c) and CD122 (IL-2/IL15Rβ) (**Figure 6A**), while the differences were more modest in $CD56^{bright}$ NK cells (**Supplemental Figure**

6A). We next asked whether iCD8α+ NK cells had greater upregulation of IL-15R components in response to IL-15, or whether existing heterogeneity in IL15R expression led to the upregulation of CD8α in cells with higher expression of IL-15R. Indeed, we found that sorted CD8α- NK cells originating from a high CD122 density had greater proliferation and upregulation of CD8α, as opposed to those originating from a CD122 low group (**Figure 6, B and C**). This indicates that NK cells with higher expression of IL15R components preferentially upregulate CD8α and expand in the presence of IL-15. IL-15 is the main driver of NK cell proliferation via signaling through three pathways: JAK1,3/STAT5, Ras/Raf/Mek/Erk (MAPK), and PI3K/AKT/mTOR. Supporting this, NK cells with higher expression of CD122/IL-15Rβ had greater resting and IL-15 induced levels of pERK and pS6 (**Supplemental Figure 6B),** while there were no significant differences in total protein levels of STAT5, ERK, AKT, or S6 (**Supplemental Figure 6C**). Thus, increased expression of the IL-15R expression corresponds to enhanced responses to IL-15 signaling. As such, we hypothesized that the enhanced expression of IL-15R components in iCD8α+ NK cells could lead to distinct responses to IL-15 signals that could be driving the observed proliferation differences. To identify signaling differences, NK cells were briefly cytokine-starved prior to stimulation with various concentrations of IL-15 for 1 hour, and phosphorylation of downstream mediators of IL-15 signaling were determined by intracellular flow cytometry. In unsorted, freshly isolated $CD56^{bright}$ NK cells gated on CD8α expression, there were modest differences in the induction of pSTAT5, pERK1/2, and pAKT, while the induction of pS6 was significantly higher in CD8α- $CD56^{bright}$ NK cells (**Supplemental Figure 6D**). Within unsorted $CD56^{dim}$ NK cells, there was a modest but consistently greater induction of pERK1/2, pAKT, and pS6 in CD8α- $CD56^{dim}$ NK cells (**Supplemental Figure 6E**). However, when controlling for the timing of CD8α acquisition using sorted CD8α- $CD56^{dim}$ NK cells, we identified greater pERK1/2, pSTAT5, pAKT, and pS6 phosphorylation (by MFI and fold change), in iCD8α+, compared to 'sustained' CD8α+ or 'persistent' CD8α- $CD56^{dim}$ NK cells (**Figure 6, D-G**). Interestingly, within sorted CD8α- $CD56^{bright}$ NK cells, both iCD8α+ and 'persistent' CD8α- subsets had greater induction of pSTAT5, pAKT, and pS6 compared to 'sustained' CD8α+ $CD56^{bright}$ NK cells (**Supplemental Figure 7, A-D**). These data suggest that the temporal dynamics of IL-15 driven expansion of IL-15R high NK cells and enhanced IL-15 signals, marked by subsequent upregulation of CD8α, are a key determinant of proliferative capacity.

Induced CD8α expression is associated with metabolic activity in NK cells

The signaling pathways downstream from the IL-15R drive transcriptional and metabolic programs that control NK cell development, homeostasis, proliferation, and function (14, 19, 52). In particular, IL-15-induced mTOR activation is a key driver of NK cell proliferation via upregulation of nutrient receptors and proteins involved in glycolysis and lipid synthesis (19, 53). As such, we hypothesized that observed differences in IL-15 signaling strength could translate to enhanced metabolic activity and drive proliferation of iCD8α+ NK cells. We identified that iCD8α+ CD56^{dim} NK cells had dramatically higher expression of CD98 (amino acid receptor component), CD71 (transferrin receptor), and GLUT1 (glucose receptor), compared to 'sustained' CD8α+ or 'persistent' CD8α- CD56^{dim} NK cells (**Figure 7A**). In CD56^{bright} NK cells, expression of CD71 was higher in iCD8α+ NK cells, but not CD98 or GLUT1, possibly due to the fact that these proteins are highly expressed by nearly all CD56^{bright} NK cells following IL-15 culture (**Supplemental Figure 8, A-C**). Consistent with the elevated expression of GLUT1 in CD56^{dim} NK cells, we identified greater uptake of the fluorescent glucose analog, 2-NBDG, in iCD8α+ NK cells, suggesting an enhanced capacity for glycolytic activity (**Figure 7B**). To further interrogate the metabolic activity of these cells, we performed Seahorse extracellular flux assays on sorted CD8α- and CD8α+ CD56^{dim} NK cells, with the caveat that these assays preclude the ability to differentiate "iCD8α+ and persistent CD8α- NK cells from the sorted CD8α- group, although flow cytometry staining was performed at the conclusion of the assay to confirm CD8α induction in the CD8α- group **(Figure 7C)**. We found that sorted CD8α- CD56^{dim} NK cells had significantly higher glucose metabolism, glycolytic capacity, and spare glycolytic reserve compared to sorted CD8α+ CD56^{dim} NK cells, suggesting a greater ability to engage in glucose-driven metabolic activity (**Figure 7D**). Additionally, we compared mitochondrial oxygen consumption rates (OCR) and observed that sorted CD8α- CD56^{dim} NK cells had greater maximal respiration and spare respiratory capacity, compared to sorted CD8α+ CD56^{dim} NK cells (**Supplemental Figure 9A**). The extent of CD8α upregulation in the sorted CD8α- CD56^{dim} group was positively correlated with higher glycolytic capacity (**Figure 7E**) but not maximal respiration **(Supplemental Figure 9B)**. These data suggest that the enhanced proliferative capacity previously identified in sorted CD8α- NK cells is primarily driven by the iCD8α+ NK cells, which are more readily able to uptake surrounding nutrients and upregulate the required glycolytic and oxidative machinery to engage in robust proliferation.

Induction of CD8α corresponds to enhanced in vitro and ex vivo responses to tumors

We next sought to determine whether this enhanced responsiveness to IL-15 signals and capacity for proliferation would translate to superior tumor control. Indeed, we found iCD8α+ NK cells had greater activation evidenced by surface CD107a, and intracellular IFNγ and TNF, following brief in vitro stimulation with K562 and HL60 leukemic cell lines (**Figure 8A-C**). To determine whether iCD8α+ NK cells retained their enhanced functionality over longer time periods, we injected sorted CD8α+ and CD8α- $CD56^{dim}$ NK cells into NSG mice, supported with IL-15, and infused with K562 tumor cells the following day (**Figure 8D**). Surprisingly, even after almost 3 weeks controlling tumors in vivo, iCD8α+ NK cells remained hyperfunctional to stimulation, and had higher expression of IFNγ and CD107a when re-challenged ex vivo with additional K562 cells or cytokines (**Figure 8E and F**). This suggests that both the enhanced proliferation and cytotoxic function of iCD8α+ NK cells mechanistically contribute to the observed differences in tumor control (**Figure 1**) in this in vivo NSG mouse model.

CD8α does not impact proliferation or apoptosis

We next sought to determine whether CD8α itself could play a functional role in regulating proliferation or survival, as CD8α homodimers have been described in intraepithelial lymphocytes (54). In agreement with previous reports (31, 34), we observed that brief CD8α ligation with two mAb clones (RPA-T8 and SK1) induced intracellular calcium flux in a flow cytometry-based assay (**Supplemental Figure 10A**). Additionally, ligating CD8α induced phosphorylation of PLCγ2, Lck, and S6, but not ZAP70/Syk, AKT, or ERK1/2 (**Supplemental Figure 8, B and C**). This signaling induction was present in control, but not CD8 KO cells (NK cells electroporated with CRISPR-Cas9 mRNA and guide RNA targeting *CD8A*), confirming that this effect was not due to non-specific antibody binding interactions. Despite the ability of CD8α to induce active signaling, we were unable to identify any impact of CD8 KO on survival or apoptosis in culture with IL-15. (**Supplemental Figure 10, D-F**). This indicates that CD8α does not intrinsically impact the ability of NK cells to expand in culture with IL-15.

CD8α restricts NK activating receptor function

CD8αα has been described on T cells to act as a TCR corepressor and on NK cells as a coreceptor that can enhance KIR clustering and binding to its cognate HLA-I ligand (26). Given that the cytoplasmic tail of CD8α can associate with Lck, a src-kinase that has been implicated in phosphorylation of both NK activating and inhibitory receptors (55), we next sought to determine if CD8α instead played a role in modulating NK cell effector function. We found that CD8 KO had minimal impact on responses to cytokines or HL60 cells, but led to modestly higher degranulation (CD107a) and TNF production against K562 leukemia cells (**Supplemental Figure 11A**). We also did not observe an impact on specific lysis of either K562 or HL60 tumor targets (**Supplemental Figure 11, B and C)** in a short-term (6 hour) killing assay. K562 cells are sensitive to NK cell killing because they lack HLA-class I expression, and express multiple activating receptor ligands, so we hypothesized that CD8α could tune the activity of specific activating receptors. We briefly stimulated control or CD8 KO primary NK cells with plate-bound antibodies directed towards activating receptors with shared (CD16, NKp30, NKp46), and distinct (CD2, CD226, 2B4, NKG2D) signaling adaptors, and measured degranulation (CD107a) and cytokine production (IFNγ, TNF). Notably, we found that CD8 KO led to significantly higher expression of IFNγ, TNF, and CD107a following stimulation with NKp30 (**Figure 9, A-C)**, and to a lesser extent 2B4, compared to control NK cells (**Supplemental Figure 12, A-C**). The impact on other activating receptors such as CD16 and CD2 was subject to greater donor to donor variability. Since CD8 KO had the greatest impact on NKp30 ligation, we focused on its interactions with this receptor. CD8α lacks a palmitoylation site that allows association with lipid rafts (56) and it has been proposed that CD8α could sequester Lck away from participating in proximal signaling events (26, 57). Successful activation of NK cells and target cell killing involves the recruitment and localization of activating receptors and the polarization of perforin-containing granules at an activating synapse (58). We therefore hypothesized that CD8α would be localized outside of these synapses. Unexpectedly, CD8α was not excluded from synapses formed against K562 or HL60 target cells, and trended towards being enriched in these synaptic areas (**Supplemental Figure 13, A and B**). We were also unable to detect robust differences in the ability to signal through activating receptors, as measured by intracellular flow cytometry assessment of key phosphorylated signaling molecules (ZAP70, PLCγ2, S6, ERK1/2, Lck, AKT) (**Supplemental Figure 14)** following activating receptor ligation in control or CD8 KO cells. Interestingly, in $CD56^{dim}$ NK cells, CD8 KO led to a modest increase in pPLCγ2, pLck, pZAP70, and pAKT following CD16 ligation, compared to control NK

cells, but we were unable to detect robust signaling following NKp30 ligation with this approach. Given the technical difficulties in capturing the kinetics of many signaling proteins at a single snapshot in time using phosphoflow, we used calcium flux to provide an integrated assessment of signaling. Since Lck has also been implicated in phosphorylating the ITIMs of KIR (55, 59, 60), and KIR and CD8α bind to non-overlapping regions of HLA (61, 62), we hypothesized that instead of suppressing activating receptor function, CD8α could be enhancing the inhibitory function of KIR. Interestingly, we found that while CD8 KO had no impact on calcium flux following NKp30 ligation alone**,** CD8 KO cells were less sensitive to KIR-mediated inhibition of NKp30, suggesting that the presence of CD8α facilitates KIR function (**Figure 9, E and F**). Together, these data suggest that CD8α can play an inhibitory role on NK cell function, likely due to its effects on KIR-mediated inhibitory signaling rather than direct modulation of activating receptor function.

Discussion

Here, we show that sorted CD8α- CD56^{dim} NK cells have superior tumor control in vivo, likely due to enhanced IL-15-induced proliferation. This phenotype was not clearly linked to terminal maturation, as CD8α expression was highest on KIR+ CD56^{dim} NK cells regardless of maturation or licensing status and there were few transcriptional differences between CD8α+ or CD8α- cells within CD56^{bright} and CD56^{dim} NK cells subsets. Interestingly, we observed that CD8α expression is dynamic, and in the presence of IL-15, a subset of sorted CD8α- NK cells induce CD8α expression while the majority remain CD8α-, and CD8α+ NK cells maintain CD8α expression once it has been established. Further analysis of the 'induced' CD8α+ (iCD8α+) subsets revealed that they drive the majority of the enhanced proliferation previously identified in sorted CD8α- CD56^{dim} NK subsets. Deletion of *CD8A* with CRISPR-Cas9 had no impact on proliferation or survival, suggesting that the intrinsic function of CD8α was unrelated to this enhanced IL-15 induced functionality. Mechanistically, iCD8α+ NK cells had greater expression of IL-15Rβ and γ receptor subunits, which resulted in significantly higher activation of the STAT5 and PI3K/AKT/mTOR pathways following IL-15 stimulation, compared to sustained CD8α+ and persistent CD8α- subsets. Interestingly, rather than IL-15-induced upregulation of IL15R components, existing heterogeneity in IL15R expression led to a preferential expansion and upregulation of CD8α in NK cells that have high expression of IL15Rβ. These enhanced signals translated to greater glucose uptake and expression of nutrient receptors in iCD8α+ NK cells, suggesting that the iCD8α+ NK cells were responsible for the higher levels of glycolysis and oxidative phosphorylation seen in sorted CD8α- NK cells.

IL-15 mediated upregulation of CD8α expression on NK cells was at least partially controlled by the transcription factor RUNX3, which has been implicated in IL-15-induced activation and proliferation of murine NK cells, and in regulating CD8α expression in T cells (63, 64). We found that RUNX3 expression was higher on iCD8α+ NK cells in IL-15 culture, and that RUNX3 knockout via CRISPR-cas9 resulted in the loss of CD8α expression in CD8α+ sorted cells, and a restricted ability of CD8α- NK cells to upregulate CD8α. This effect was specific to CD8α, and not CD8β. Further, using CUT&TAG we found that RUNX3 modulates H3K27ac abundance within the *CD8A* locus, supporting a direct role for RUNX3 in regulating CD8α expression. Notably, RUNX3 also

regulated expression of several KIR genes, in addition to genes related to NK cell activation and translation initiation / nutrient transport, suggesting RUNX3 may facilitate the enhanced proliferation and effector function of induced CD8α+ NK cells. However, given that RUNX3 can form a heterodimer with CBFβ and has also been described to act in concert with TBET, further work should be done to determine the contribution of other transcription factors to CD8α expression (64, 65). Future studies interrogating other epigenetic modifications such as H3K4me3 and transcriptional activators, such as Mediator, may further elucidate the transcriptional program regulated by RUNX3 and whether it directly or indirectly regulates CD8α and other IL-15-induced transcriptional programs.

In addition to the role of IL-15 in driving NK cell survival and proliferation, it has been demonstrated that IL-15 induced glucose metabolism is required for NK cell effector function (22). Consistent with this, the amino-acid sensing CD98-mTOR pathway has been shown to be critical for NK cell metabolism and effector function (66, 67). Our observation that iCD8α+ NK cells have greater upregulation of nutrient receptors suggests that they have improved metabolic support for enhanced proliferation and anti-tumor effector function. Consistent with this, we found that iCD8α+ NK cells have higher functionality against both the HLA-deficient K562 cell line, and the HLA-sufficient HL60 cell line, suggesting that the presence or absence of HLA on a target cell does not necessarily impact this enhanced functionality. We also found that sorted CD8α- NK cells had a superior ability to control tumors in vivo, likely due to the enhanced proliferation and durable functionality of iCD8α+ NK cells, as opposed to those that were sorted CD8α+ and sustained CD8α expression.

Altogether, these data suggest that our previous observation that patients treated with ML NK cells with higher initial CD8α expression failed treatment could result from the hypofunctionality of ‘sustained’ CD8α+ NK cells (24). Surprisingly, even after almost three weeks in vivo in the presence of K562 tumor cells and high doses of IL-15, iCD8α+ NK cells had enhanced responses to K562 and cytokine stimulation, compared to persistent CD8α- or sustained CD8α+. This suggests that the loss of functionality associated with sustained CD8α+ expression occurs at time points that are far beyond the half-lives of adoptively transferred NK cells, or is driven by additional tissue-specific factors not evaluated (68).

The CD8αα homodimer has been described to act as a TCR corepressor that can decrease the TCR functional avidity, thus increasing the signal strength required for T cell activation (69, 70). Indeed, studies in intraepithelial lymphocytes (IEL) have demonstrated that CD8αα binding to thymus leukemic antigen (TL) restricts IEL proliferation and activation (71). Since the CD8α cytosolic tail binds the Src-kinase Lck, and lacks the palmitoylation site that allows close association with lipid rafts (56, 72, 73), Lck sequestration is proposed to be important for CD8αα inhibitory activity. Interestingly, Lck is also required for the phosphorylation of the ITIM domains of inhibitory KIR that are clustered at the immune synapse (55, 60, 62) thus facilitating recruitment of the phosphatases SHP-1 and SHP-2 (74, 75). As such, it is also possible that CD8α binding to HLA class I in concert with KIR can modulate NK cell activity. It was reported that the CD8αα can function as a coreceptor that enhances KIR clustering and binding to its cognate HLA-I ligand on adjacent NK cells, thereby increasing the inhibitory effect of KIRs (36). In this study, we identified that CRISPR-Cas9 knockout of *CD8A* in primary human NK cells leads to enhanced NK cell degranulation and cytokine secretion following ligation with various activating receptors, particularly NKp30. Interestingly, we could not identify any direct impact of CD8α on activating coreceptor signaling, but rather a decreased sensitivity to KIR-mediated inhibition in the absence of CD8α. Notably, we found that CD8α expression was enriched on KIR+ NK cells. Therefore, we propose a model whereby IL-15 stimulation induces robust NK cell proliferation, metabolic activity, and cytotoxic functional capacity that is marked by CD8α expression, which subsequently acts as a rheostat to tune the threshold to release KIR-mediated inhibition and prevent aberrant activation. This finding is consistent with a potential role for CD8α as a coreceptor for KIR3DL1 on NK cells, though further work is required to define the exact mechanism by which CD8α functions, and whether this extends to other members of the KIR family. We hypothesize that after sufficient IL-15 signaling and time, iCD8α+ NK cells may transition to a phenotype that more closely resembles ‘sustained CD8α+’ NK cells. To that end, the impaired functionality of “sustained CD8α+” NK cells may be two-fold – as a consequence of an exhaustion-like state from chronic stimulation (manifesting in reduced responses to IL-15 signaling and lesser functional responses), and due to high expression of CD8α (tuning NK cell activation). In the context of responses against HLA-deficient K562s, the former effect may predominate, while against HLA-expressing cells it may be a combination of the two. Notably, the per-cell expression of CD8α (as measured by MFI) on iCD8α+ NK cells is much lower than that of “sustained CD8α+” NK cells, suggesting

that iCD8α+ NK cells are at least transiently less susceptible to inhibitory effects of CD8α. Finally, while K562s lack HLA expression, it is also possible that some level of tonic inhibition is tumor-target independent, and is mediated by NK:NK interactions of CD8α/KIR-HLA.

In summary, this study reveals that CD8α expression on NK cells marks a spectrum of functionality, whereby recent induction of CD8α expression by CD8α- NK cells corresponds with robust proliferation, metabolic activity, and functional responses. CD8α- NK cells, which can remain CD8α- or become iCD8α+, mediate superior tumor control in leukemia-xenograft mouse models, likely due to their enhanced capacity for expansion in vivo. This enhanced functionality is lost over time, as sustained expression of CD8α is associated with hypofunctionality. Finally, this study identifies a functional, inhibitory role for CD8α in regulating NK cell function. These findings highlight the importance of interrogating the dynamics of NK cell marker acquisition as they relate to functionality, particularly in the context of understanding NK cell biology and improving cellular therapies.

Methods

Lead Contact and Materials Available

Further information and requests for resources and reagents should be directed to and will be fulfilled by the lead contact, Todd A. Fehniger (tfehnige@wustl.edu).

Sex as a biological variable

Experiments were performed on male and female mice that were age and sex matched within experiments. No differences between sexes were observed.

CRISPR-Cas9 gene editing

NK cells were purified from normal donors and rested overnight in HAB10 with 1 ng/mL IL15. Cells were washed with PBS two times to remove serum, and resuspended in MaxCyte EP buffer plus Cas9 mRNA (Trilink). Next, CD8A sgRNA (GACUUCCGCCGAGAGAACGA), [IDT with modifications as described previously (76)], *RUNX3* sgRNA (UGCGCACGAGCUCGCCUGCG) or control sgRNA against the TCRα chain, TRAC (GAGAAUCAAAAUCGGUGAAU) (Synthego) was added to the cells, which were then electroporated in a Maxcyte GT electroporator using the WUSTL-2 setting in an OC-100 processing assembly. Cells were removed from the OC-100 and incubated for 10 minutes at 37°C. Pre-warmed media containing 1 ng/mL IL15 was added and cells rested for 24 hours. Cells were then spun down (1300 rpm, 4 min) and resuspended at $2.5x10^6$ to $5x10^6$ cells/mL and cultured as described above. Protein knock-out was confirmed by flow cytometric staining at the indicated time point.

Antibody cross-linking phosphorylation assays

Six days following electroporation and culture in HAB10 + 1 ng/mL IL-15, control or CD8 KO NK cells were plated at approximately $2.0x10^5$ to $2.5x10^5$ cells/well of a round bottom 96-well plate in HAB10 containing 1 ng/mL rh-IL-15. Monoclonal antibodies directed against the indicated activating receptors were added at 10 µg/mL, and incubated for 20 min at 4°C. Following incubation, cells were spun down at 1800 rpm for 4 min, and resuspended in HAB10 containing 20 µg/mL goat anti-mouse IgG to induce cross-linking for 5 min at 37°C. After incubation,

cells were fixed with 4% PFA, permeabilized with methanol, and stained for flow cytometry analysis as described above.

CUT&TAG data generation and analysis

Freshly isolated NK cells were electroporated with RUNX3 or control (TRAC) sgRNA and Cas9 mRNA as described above, cultured in 5 ng/mL IL-15 for 9 days, and assessed for H3K27ac abundance using the Active Motif CUT&Tag-IT anti-Rabbit assay kit. For each condition, 500,000 fresh, whole cells were used. RUNX3 knockout efficiency of ~70-80% was validated by flow cytometry on the day of sample preparation. Resulting libraries were submitted to the Washington University McDonnell Genome Institute for sequencing on the Illumina NovaSeq 6000 instrument. For analysis, CUT&TAG fastq files were aligned and analyzed using a pipeline adapted from [(77–79)] using bowtie2, samtools, bedtools, and SEACR. H3K27ac bedgraph files for control and RUNX3 knockout (KO) were compared to donor-matched IgG bedgraph files to identify H3K27ac peaks. Genome annotation of peaks was performed with ChIPseeker using promoter = +/- 3kb and assigning nearest gene to each peak; 9558 genes had peaks assigned. Statistical analyses, filtering, and data visualization were performed using R. Total signal in peaks assigned to genes was compared between control and KO conditions for each donor using matched paired t-tests and log2 fold change. We filtered genes $p<0.05$ using the results of one-sided t-tests (peaks lost/lower in KO or peaks gained/higher in KO), log2 fold change $\leq$ -0.5 or $\geq$ 0.5, respectively) in least 3 of 4 donors, for genes expressed in NK cells. This strategy identified 174 genes with lost or lower peaks in KO and 23 genes with gained or higher peaks in KO. Data has been uploaded to GEO under accession number GSE263686.

Calcium Flux assays

Calcium flux assays were performed by washing freshly isolated human NK cells with pre-warmed MCF media (HBSS with calcium [Thermo Fisher Scientific], 1% 1M HEPES [Thermo Fisher Scientific], and 2% human serum) and incubating NK cells with indo-1, AM (Thermo Fisher Scientific), a UV-light excitable Ca^{2+} indicator (emission maximum of indo-1 shifts from ~475 nM in Ca^{2+} -free medium to ~400 nM when the dye is saturated with Ca^{2+}) for 30 min at 37°C, with mixing performed every 10 minutes. Indo-1 labeled cells were washed, resuspended with 10 µg/mL of monoclonal antibody or mIgG1 isotype control, and incubated at 37°C for 15 min. Cells were washed and resuspended in MCF media, and rested for 37°C for at least 15 minutes prior to acquisition on a

UV-laser equipped FACS ARIA II on a flow rate of ~2000 events/s for 15 seconds. Acquisition was paused, 20 µg/mL goat anti-mouse IgG was added to induce cross-linking, cells were vortexed, and acquisition was resumed for 5 minutes. Data analysis was performed by comparing the ratio of the median fluorescence intensity of indo-blue and indo-violet over the time series, and normalized to the first reading, using FlowJo Version 10.8.1 (TreeStar) software.

NSG xenograft model and BLI imaging

Approximately $1x10^6$ to $2x10^6$ CD8α+ or CD8α - $CD56^{dim}$ NK cells were injected intravenously (tail-vein) into NSG mice. The next day, 0.4 $x10^6$ to $0.5x10^6$ K562-luciferase expressing cells were injected intravenously (tail-vein). NK cells were supported with intraperitoneal (i.p.) 1 µg / mouse rh-IL-15 3x/week, and tumor measurements were assessed via bioluminescent imaging (BLI) on Days 1, 4, 7, 11, and 15 post tumor injection. All mice were irradiated with 125cGys one day before NK cell injection. For each treatment condition, sorted NK cells were injected into 1-2 mice each, and the data point for each donor / condition was calculated as an average of the photons within a fixed ROI of the dorsal and ventral side of each mouse, for each mouse used (i.e. data point for one donor and one condition was an average of the measurements from two separate mice, for a total of 5 unique donors and 8-10 mice total per condition). Experiments were performed on 8 to 10 week old mice that were age and sex matched within experiments. All mice were maintained and used in accordance with our animal protocol approved by the Washington University Animal Studies Committee. BLI imaging was performed on an IVIS 50 (10–90 s exposure, bin8, field of view [FOV] 12 cm, open filter) (Xenogen, Alameda, CA). Mice were injected i.p. with D-luciferin (150 mg/kg in PBS, Gold Biotechnology, St. Louis, MO) and imaged under anesthesia with isoflurane (2% vaporized in O_2). Total photon flux (photons/s) was measured from fixed regions of interest over the entire mouse (average of dorsal and ventral images) using the Living Image 2.6 software program.

Confocal immunofluorescence microscopy and image analysis

For fixed cell confocal imaging, freshly isolated primary human NK cells were co-cultured with K562 or HL60 target cells at a 2:1 effector to target ratio in HAB10 media with 1 ng/mL IL-15 for 30 minutes at 37°C in 5% CO_2. Cells were gently pipetted to remove clumps, then transferred to poly-L-lysine (0.01%) coated 8-well chambers

(#1.5) for an additional 30 minutes at 37°C. After incubation, cells were fixed and permeabilized with CytoFix/CytoPerm (BD Biosciences) at 4°C for 20 minutes, then washed with PBS and permeabilized with PBSS (1x PBS, 1% bovine serum albumin, 0.1% saponin). Conjugate staining was performed at 4°C overnight in PBSS using phalloidin AF555 (Life Technologies), CD8a FITC (clone HIT8A) and perforin bv421 (clone dG9) (BioLegend). After staining, cells were washed and covered with vectashield mounting medium (Vector Laboratories). Images were acquired using a Nikon AXR Confocal Microscope with the 60X oil immersion objective (Washington University Center for Cellular Imaging, WUCCI), on a Ti2 microscope stand, using an 8k galvo scanner. Data were exported as ND2 files for further analysis. Fiji (version 1.54) was used to process and analyze confocal images (80). After identification of NK:tumor conjugates, the z-slice with optimal perforin polarization and actin accumulation at the synapse was used for quantification of the fluorescence intensity of actin and CD8α. Regions of interest were drawn within synaptical and non-synaptical (distal end) membrane regions of the NK cell, and fluorescence intensity of actin or CD8α was calculated as the ROI area (um^2) x the mean of fluorescence intensity, for each individual cell.

Statistics

Statistical comparisons were performed as indicated in each figure using GraphPad Prism (v10) software. Data are represented as mean ± SEM, and all significance testing comparisons are 2-sided. The specific statistical tests and the sample size are indicated in the respective figure legends. $P < 0.05$ was considered statistically significant.

Study Approval

All animal studies were approved by the Washington University IACUC (St. Louis, MO) and experiments were conducted in accordance with the guidelines of and with approval by the Washington University Animal Studies Committee.

Data and Code Availability

Bulk RNA sequencing and CUT&TAG data are available using GEO accession numbers GSE236394 and GSE263686, respectively. For single cell RNA sequencing data, healthy donor purified NK cells were used (dbGaP Study Accession: phs002681) (81). Values for all data points in graphs are reported in the Supporting Data Values file.

Author Contributions

Conceptualization: CCC, TAF; Methodology: CCC, MMB-E, TAF, EMM; Investigation and Formal Analysis: CCC, PW, HKD, JAF, JT, LM, MF, KH, NDM, TS, HF, MB-H, AYZ, MTJ, DAR-G, EM, MMB-E, JEP; Writing – original draft: CCC, TAF; Writing – review and editing: all authors.

Acknowledgments

We thank Megan Cooper for insightful discussion. This work was supported by NIH/NIAID F30AI161318 to CCC. NIH/NCI R01CA205239 to TAF, NIH/NCI P50CA171963 to T.A.F. and MMB-E, NIH/NCI P30CA91842 to T.A.F. NIH/NIGMS: T32GM139799 to JAF. NIH/NIGMS: F31GM146361 to JT. NIH/ NHLBI T32HL007088 to PW. NIH-NIAID R01AI13030 to EMM. NIH 5K12CA167540 to MMB-E. This work was also supported in part by the Paula C. and Rodger O. Riney Blood Cancer Research Initiative. We thank the Genome Technology Access Center at the McDonnell Genome Institute at Washington University School of Medicine for help with genomic analysis.

Declaration of Competing Interests

Conflict of interest: TAF and MMB-E have pending patents (15/983,275; 62/963,971, and PCT/ US2019/060005) licensed to Wugen Inc., equity interest, consulting for, and royalty interest in Wugen Inc unrelated to this work. JAF has pending patents (WO 2019/152387, US 63/018,108) unrelated to the present work that are licensed to Kiadis, and a monoclonal antibody unrelated to the present work licensed to EMD Millipore. MB-H has patent (US8895020B2) unrelated to the present work. Unrelated to this work, CCC has equity in Pionyr Immunotherapeutics, and DAR- G receives consulting fees from Cartography Inc. TAF reports research funding from the NIH during the conduct of the study; equity, research funding, consulting fees from Wugen, Inc., research funding from ImmunityBio, HCW Biologics and Affimed, consulting fees from Kiadis, Takeda, AI Proteins, Smart Immune, Affimed, and other support from Indapta and OrcaBio, all unrelated to this work.

References

1. Caligiuri MA. Human natural killer cells. *Blood* 2008;112(3):461–469.
2. Yokoyama WM, Kim S, French AR. The Dynamic Life of Natural Killer Cells. *Annu. Rev. Immunol.* 2004;22(1):405–429.
3. Cerwenka A, Lanier LL. Natural killer cells, viruses and cancer. *Nat. Rev. Immunol.* 2001;1(1):41–49.
4. Cooper MA, Fehniger TA, Caligiuri MA. The biology of human natural killer-cell subsets.. *Trends Immunol* 2001;22(11):633–40.
5. Lanier LL. NK cell recognition.. *Ann Rev Immunol* 2005;23(1):225–74.
6. Long EO, et al. Controlling Natural Killer Cell Responses: Integration of Signals for Activation and Inhibition. *Annu. Rev. Immunol.* 2013;31(1):227–258.
7. Wagtmann N, et al. Killer cell inhibitory receptors specific for HLA-C and HLA-B identified by direct binding and by functional transfer. *Immunity* 1995;3(6):801–809.
8. Brooks AG, et al. NKG2A Complexed with CD94 Defines a Novel Inhibitory Natural Killer Cell Receptor. *J. Exp. Med.* 1997;185(4):795–800.
9. López-Botet M, et al. The CD94/NKG2 C-type lectin receptor complex. *Immunol. Res.* 1997;16(2):175–185.
10. Moretta A, et al. Activating Receptors and Coreceptors Involved in Human Natural Killer Cell-Mediated Cytolysis. *Annu. Rev. Immunol.* 2001;19(1):197–223.
11. Vivier E, Nunès JA, Vély F. Natural killer cell signaling pathways. *Science (80-.).* 2004;306(5701):1517–1519.
12. Bell GM, et al. The SH3 domain of p56lck binds to proline-rich sequences in the cytoplasmic domain of CD2. *J. Exp. Med.* 1996;183(1):169–178.
13. Lanier LL. Natural killer cell receptor signaling. *Curr. Opin. Immunol.* 2003;15(3):308–314.
14. Fehniger TA, Caligiuri MA. Interleukin 15: biology and relevance to human disease. *Blood* 2001;97(1):14–32.
15. Carson WE, et al. A potential role for interleukin-15 in the regulation of human natural killer cell survival. *J. Clin. Invest.* 1997;99(5):937–943.
16. Carson WE, et al. Interleukin 15 is a novel cytokine that activates natural killer cells via components of

the IL-2 receptor. *J Exp Med* 1994;180:1395–1403.

17. Rautela J, Huntington ND. IL-15 signaling in NK cell cancer immunotherapy. *Curr. Opin. Immunol.* 2017;44:1–6.
18. Waldmann TA. The biology of interleukin-2 and interleukin-15: implications for cancer therapy and vaccine design.. *Nat Rev Immunol* 2006;6(8):595–601.
19. Marçais A, et al. The metabolic checkpoint kinase mTOR is essential for IL-15 signaling during the development and activation of NK cells.. *Nat. Immunol.* 2014;15(8):749–57.
20. Powell JD, et al. Regulation of Immune Responses by mTOR. *Annu. Rev. Immunol.* 2012;30(1):39–68.
21. Keating SE, et al. Metabolic Reprogramming Supports IFN-γ Production by CD56 bright NK Cells . *J. Immunol.* 2016;196(6):2552–2560.
22. Mah AY, et al. Glycolytic requirement for NK cell cytotoxicity and cytomegalovirus control. *JCI Insight* 2017;2(23):1–17.
23. Kieffer LJ, et al. Human CD8α expression in NK cells but not cytotoxic T cells of transgenic mice. *Int. Immunol.* 1996;8(10):1617–1626.
24. Berrien-Elliott MM, et al. Multidimensional Analyses of Donor Memory-Like NK Cells Reveal New Associations with Response after Adoptive Immunotherapy for Leukemia. *Cancer Discov.* 2020;10(12):1854–1871.
25. Baume DM, et al. Differential expression of CD8α and CD8β associated with MHC-restricted and non-MHC-restricted cytolytic effector cells. *Cell. Immunol.* 1990;131(2):352–365.
26. Cheroutre H, Lambolez F. Doubting the TCR Coreceptor Function of CD8αα. *Immunity* 2008;28(2):149–159.
27. den Haan JMM, Lehar SM, Bevan MJ. Cd8+ but Not Cd8− Dendritic Cells Cross-Prime Cytotoxic T Cells in Vivo. *J. Exp. Med.* 2000;192(12):1685–1696.
28. Leishman AJ, et al. T cell responses modulated through interaction between CD8alphaalpha and the nonclassical MHC class I molecule, TL.. *Science* 2001;294(5548):1936–9.
29. Goodall KJ, et al. The murine CD94/NKG2 ligand, Qa-1b, is a high-affinity, functional ligand for the CD8αα homodimer. *J. Biol. Chem.* 2020;295(10):3239–3246.
30. Gao GF, et al. Classical and Nonclassical Class I Major Histocompatibility Complex Molecules Exhibit

Subtle Conformational Differences That Affect Binding to CD8αα. *J. Biol. Chem.* 2000;275(20):15232–15238.

31. Lowdell MW, et al. Evidence that continued remission in patients treated for acute leukaemia is dependent upon autologous natural killer cells. *Br. J. Haematol.* 2002;117(4):821–827.
32. Ahmad F, et al. High Frequencies of Polyfunctional CD8+ NK Cells in Chronic HIV-1 Infection Are Associated with Slower Disease Progression. *J. Virol.* 2014;88(21):12397–12408.
33. McKinney EF, et al. A CD8+ NK cell transcriptomic signature associated with clinical outcome in relapsing remitting multiple sclerosis. *Nat. Commun.* 2021;12(1):635.
34. Addison EG, et al. Ligation of CD8alpha on human natural killer cells prevents activation-induced apoptosis and enhances cytolytic activity. *Immunology* 2005;116(3):354–361.
35. Spaggiari GM, et al. Soluble HLA class I molecules induce natural killer cell apoptosis through the engagement of CD8: evidence for a negative regulation exerted by members of the inhibitory receptor superfamily. *Blood* 2002;99(5):1706–1714.
36. Geng J, Raghavan M. CD8αα homodimers function as a coreceptor for KIR3DL1. *Proc. Natl. Acad. Sci.* 2019;116(36):17951–17956.
37. Miller JS, et al. Successful adoptive transfer and in vivo expansion of human haploidentical NK cells in patients with cancer.. *Blood* 2005;105(8):3051–3057.
38. Berrien-Elliott MM, Jacobs MT, Fehniger TA. Allogeneic natural killer cell therapy. *Blood* 2023;141(8):856–868.
39. Cooper MA, et al. Cytokine-induced memory-like natural killer cells.. *Proc. Natl. Acad. Sci. U. S. A.* 2009;106(6):1915–9.
40. Berrien-Elliott MM, et al. Systemic IL-15 promotes allogeneic cell rejection in patients treated with natural killer cell adoptive therapy. *Blood* 2022;139(8):1177–1183.
41. Bednarski JJ, et al. Donor memory-like NK cells persist and induce remissions in pediatric patients with relapsed AML after transplant. *Blood* 2022;139(11):1670–1683.
42. Bachanova V, et al. Clearance of acute myeloid leukemia by haploidentical natural killer cells is improved using IL-2 diphtheria toxin fusion protein. *Blood* 2014;123(25):3855–3863.
43. Wagner JA, et al. Stage-Specific Requirement for Eomes in Mature NK Cell Homeostasis and

Cytotoxicity. *Cell Rep.* 2020;31(9):107720.

44. Huntington ND, et al. Interleukin 15-mediated survival of natural killer cells is determined by interactions among Bim, Noxa and Mcl-1. *Nat. Immunol.* 2007;8(8):856–863.

45. Kim S, et al. Licensing of natural killer cells by host major histocompatibility complex class I molecules.. *Nature* 2005;436(7051):709–13.

46. Wagner JA, et al. Cytokine-Induced Memory-Like Differentiation Enhances Unlicensed Natural Killer Cell Antileukemia and FcγRIIIa-Triggered Responses. *Biol. Blood Marrow Transplant.* 2017;23(3). doi:10.1016/j.bbmt.2016.11.018

47. Stelzer G, et al. The GeneCards Suite: From Gene Data Mining to Disease Genome Sequence Analyses.. *Curr. Protoc. Bioinforma.* 2016;54:1.30.1-1.30.33.

48. Kaya-Okur HS, et al. CUT&Tag for efficient epigenomic profiling of small samples and single cells.. *Nat. Commun.* 2019;10(1):1930.

49. Budagian V, et al. IL-15/IL-15 receptor biology: A guided tour through an expanding universe. *Cytokine Growth Factor Rev.* 2006;17(4):259–280.

50. Freud AG, Caligiuri MA. Human natural killer cell development.. *Immunol Rev* 2006;214(1):56–72.

51. Poli A, et al. CD56bright natural killer (NK) cells: an important NK cell subset.. *Immunology* 2009;126(4):458–465.

52. Mao Y, et al. IL-15 activates mTOR and primes stress-activated gene expression leading to prolonged antitumor capacity of NK cells. *Blood* 2016;128(11):1475–1489.

53. Merino A, et al. Chronic stimulation drives human NK cell dysfunction and epigenetic reprograming. *J. Clin. Invest.* 2019;129(9):3770–3785.

54. Vandereyken M, James OJ, Swamy M. Mechanisms of activation of innate-like intraepithelial T lymphocytes. *Mucosal Immunol.* 2020;13(5):721–731.

55. Binstadt BA, et al. Sequential Involvement of Lck and SHP-1 with MHC-Recognizing Receptors on NK Cells Inhibits FcR-Initiated Tyrosine Kinase Activation. *Immunity* 1996;5(6):629–638.

56. Arcaro A, et al. Essential Role of CD8 Palmitoylation in CD8 Coreceptor Function. *J. Immunol.* 2000;165(4):2068–2076.

57. Gangadharan D, Cheroutre H. The CD8 isoform CD8αα is not a functional homologue of the TCR co-

receptor CD8αβ. *Curr. Opin. Immunol.* 2004;16(3):264–270.

58. Mace EM, et al. Cell biological steps and checkpoints in accessing NK cell cytotoxicity.. *Immunol. Cell Biol.* 2014;92(October 2013):245–55.

59. Treanor B, et al. Microclusters of inhibitory killer immunoglobulin–like receptor signaling at natural killer cell immunological synapses. *J. Cell Biol.* 2006;174(1):153–161.

60. Marti F, et al. LCK-phosphorylated human killer cell-inhibitory receptors recruit and activate phosphatidylinositol 3-kinase. *Proc. Natl. Acad. Sci.* 1998;95(20):11810–11815.

61. Gao GF, et al. Crystal structure of the complex between human CD8αα and HLA-A2. *Nature* 1997;387(6633):630–634.

62. Vivian JP, et al. Killer cell immunoglobulin-like receptor 3DL1-mediated recognition of human leukocyte antigen B. *Nature* 2011;479(7373):401–405.

63. Levanon D, et al. Transcription Factor Runx3 Regulates Interleukin-15-Dependent Natural Killer Cell Activation. *Mol. Cell. Biol.* 2014;34(6):1158–1169.

64. Hassan H, et al. Cd8 enhancer E8 I and Runx factors regulate CD8α expression in activated CD8 + T cells. *Proc. Natl. Acad. Sci.* 2011;108(45):18330–18335.

65. Cruz-Guilloty F, et al. Runx3 and T-box proteins cooperate to establish the transcriptional program of effector CTLs.. *J. Exp. Med.* 2009;206(1):51–59.

66. De Barra C, et al. Glucagon-like peptide-1 therapy in people with obesity restores natural killer cell metabolism and effector function. *Obesity* [published online ahead of print: May 9, 2023]; doi:10.1002/oby.23772

67. Loftus RM, et al. Amino acid-dependent cMyc expression is essential for NK cell metabolic and functional responses in mice. *Nat. Commun.* 2018;9(1):2341.

68. Zhang Y, et al. In vivo kinetics of human natural killer cells: the effects of ageing and acute and chronic viral infection. *Immunology* 2007;121(2):258–265.

69. van Oers NS, et al. CD8 inhibits signal transduction through the T cell receptor in CD4-CD8- thymocytes from T cell receptor transgenic mice reconstituted with a transgenic CD8 alpha molecule.. *J. Immunol.* 1993;151(2):777–90.

70. Cawthon AG, Lu H, Alexander-Miller MA. Peptide Requirement for CTL Activation Reflects the

Sensitivity to CD3 Engagement: Correlation with CD8αβ Versus CD8αα Expression. *J. Immunol.* 2001;167(5):2577–2584.

71. Ma H, Qiu Y, Yang H. Intestinal intraepithelial lymphocytes: Maintainers of intestinal immune tolerance and regulators of intestinal immunity. *J. Leukoc. Biol.* 2021;109(2):339–347.
72. Cawthon AG, Alexander-Miller MA. Optimal Colocalization of TCR and CD8 as a Novel Mechanism for the Control of Functional Avidity. *J. Immunol.* 2002;169(7):3492–3498.
73. Pang DJ, Hayday AC, Bijlmakers M-J. CD8 Raft Localization Is Induced by Its Assembly into CD8αβ Heterodimers, Not CD8αα Homodimers. *J. Biol. Chem.* 2007;282(18):13884–13894.
74. Burshtyn DN, et al. Adhesion to target cells is disrupted by the killer cell inhibitory receptor. *Curr. Biol.* 2000;10(13):777–780.
75. Burshtyn DN, et al. Recruitment of Tyrosine Phosphatase HCP by the Killer Cell Inhibitory Receptor. *Immunity* 1996;4(1):77–85.
76. Cooper ML, et al. An “off-the-shelf” fratricide-resistant CAR-T for the treatment of T cell hematologic malignancies. *Leukemia* 2018;32(9):1970–1983.
77. Meers MP, Tenenbaum D, Henikoff S. Peak calling by Sparse Enrichment Analysis for CUT&RUN chromatin profiling. *Epigenetics and Chromatin* 2019;12(1):1–11.
78. Meers MP, et al. Improved CUT&RUN chromatin profiling tools.. *Elife* 2019;8. doi:10.7554/eLife.46314
79. Zheng Y, Ahmad K, Henikoff S. CUT&Tag Data Processing and Analysis Tutorial2020; doi:10.17504/protocols.io.bjk2kkye
80. Schindelin J, et al. Fiji: an open-source platform for biological-image analysis. *Nat. Methods* 2012;9(7):676–682.
81. Berrien-Elliott MM, et al. Hematopoietic Cell Transplantation Donor-derived Memory-Like NK Cells Functionally Persist after Transfer into Patients with Leukemia. *Sci. Transl. Med.* 2022;14(633):eabm1375.

Figure legends:

Figure 1: CD8α- CD56^{dim} NK cells have enhanced tumor control *in vivo*

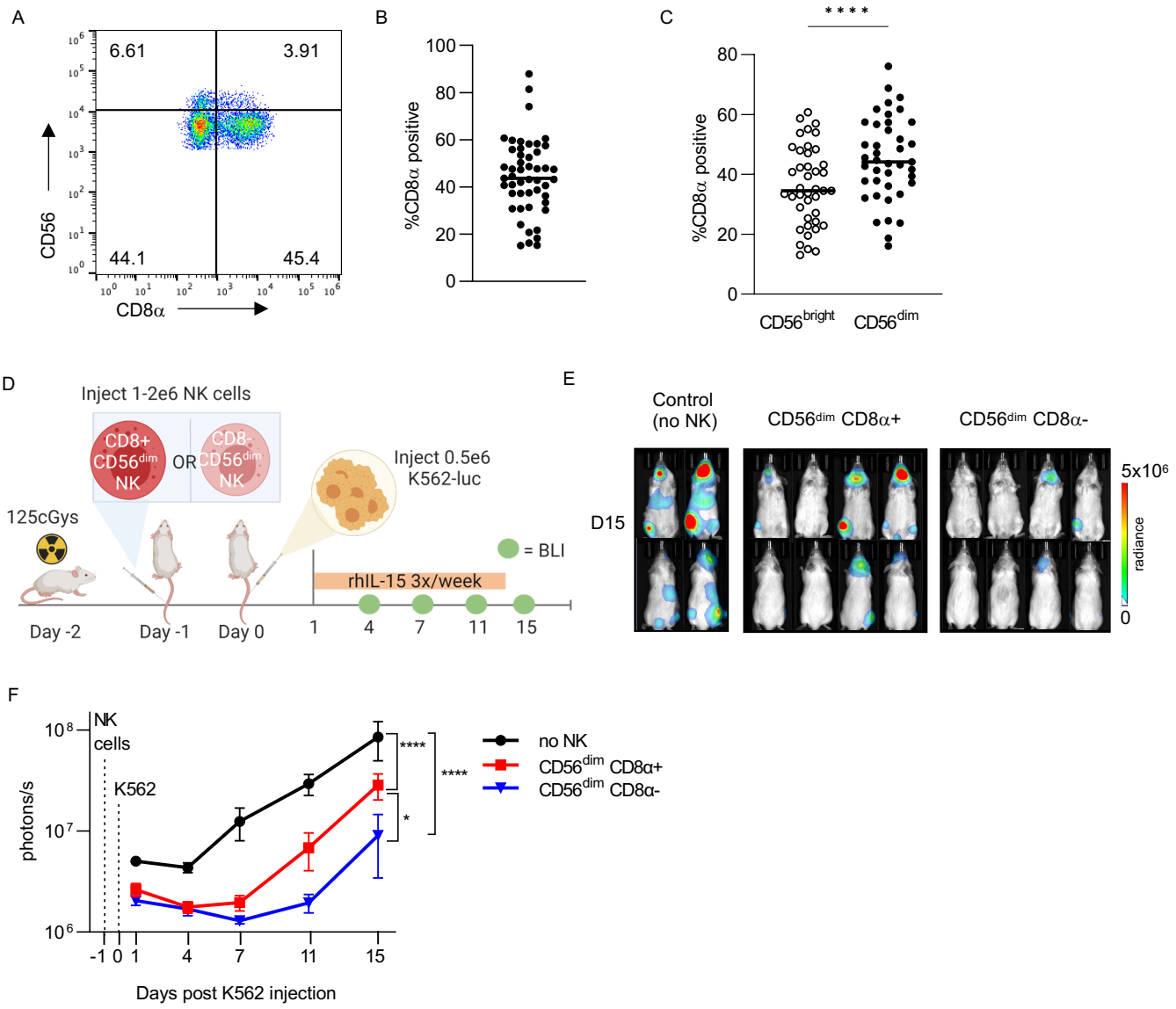

Figure 1: Sorted CD8α- NK cells have enhanced tumor control in vivo. (A) Representative flow plot showing CD8α expression on CD56^{bright} and CD56^{dim} NK cells. **(B).** Percentage of freshly isolated healthy donor human NK cells that express CD8α. **(C)** Percentage of freshly isolated NK cells, gated into CD56^{bright} or CD56^{dim}, that express CD8α. n=49. Statistical significance was determined using two-tailed paired t-test. **(D-F)** CD56^{dim} CD8α+ and CD8α– NK cells were sorted from primary human NK cells and rested overnight in 1 ng/mL IL-15. The next day, approximately 1 to 2x10^6 CD8α+ or CD8α - CD56^{dim} NK cells were injected intravenously (tail vein) into NSG mice (D-1). The following day, 0.4x10^6-0.5x10^6 K562-CBR-luc (K562-luc) cells were injected intravenously

(tail vein) (D0). NK cells were supported with intraperitoneal (i.p.) rh-IL-15 3x/week, and tumor burden was assessed via bioluminescent imaging (BLI) on Days 1, 4, 7, 11, and 15 post tumor injection. **(D)** Experimental schema. **(E)** Representative BLI images from one of 3 independent experiments on Day 15 and **(F)** summary data showing tumor burden as mean +/- SEM within the indicated groups. N=5 unique donors, 3 independent experiments, 8-10 mice within each group. Statistical significance was determined using mixed effects-model with Holm-Šídák correction for multiple comparisons. *p<0.05, **p<0.01, ***p<0.001, ****p<0.0001

Figure 2: CD8α- NK cells have enhanced proliferation and survival *in vitro* and *in vivo*

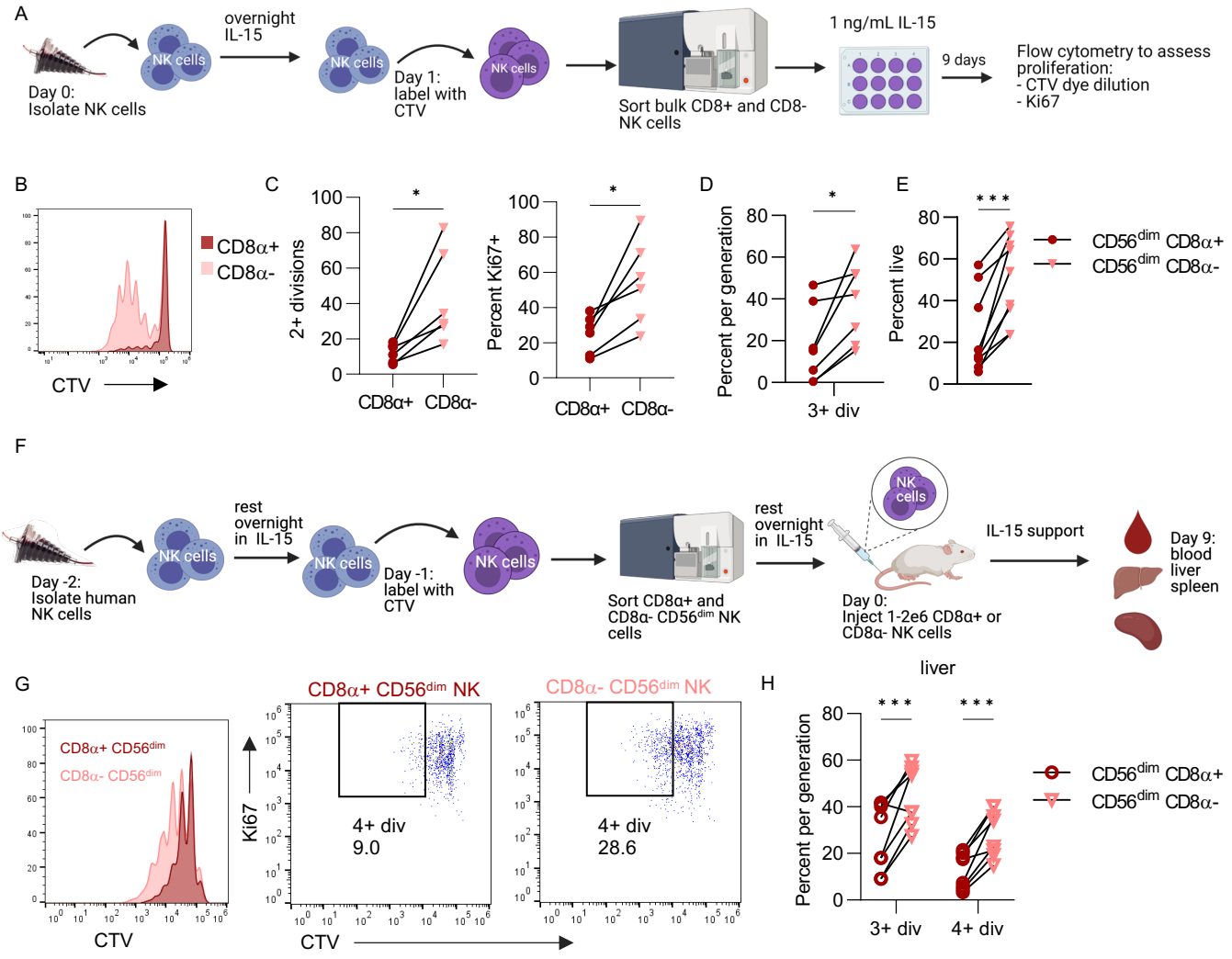

Figure 2: Sorted CD8α- NK cells have enhanced proliferation and survival in vitro and in vivo. (A-E) Freshly isolated NK cells were labeled with cell-trace violet (CTV), sorted based on CD8α expression, and cultured with 1 ng/mL IL-15 in vitro for 7 days. **(A)** Experimental schema. **(B)** Representative histogram of CTV dilution in CD8α+ and CD8α- NK cells at Day 7. Percentage of NK cells with **(C)** 2 or more divisions or Ki67 expression at D7. N= 6 donors, 3 independent experiments. **(D-E)** CD8α+ or CD8α- CD56^{dim} NK cells were labeled with CTV, sorted, and cultured in vitro in 1 ng/mL IL-15 for 9 days. **(D)** Proliferation was assessed by CTV dye dilution. Data shown as the percentage of NK cells that have undergone the indicated number of divisions. **(E)** Cell death was assessed by staining of AnnexinV and 7AAD (live = AnnexinV-, 7AAD-). N=7-9 donors, 4 independent experiments. **(F-H)** Sorted CD8α+ and CD8α- CD56^{dim} NK cells were labeled with CTV

and injected i.v. into different NSG mice. Human NK cells were supported with i.p. injections of rh-IL-15 3x/week. **(F)** Experimental schema. Proliferation was assessed by CTV dye dilution and Ki67 expression. **(G)** Representative histogram and **(H)** summary data showing the percentage of NK cells that have undergone the indicated number of divisions in the liver of NSG mice. Statistical significance was determined by (C-E) paired two tailed t-test and (H) two-way ANOVA with Holm-Šídák correction for multiple comparisons. N=9 donors, 5 independent experiments. *p<0.05, **p<0.01, ***p<0.001, ****p<0.0001.

Figure 3: CD8α does not mark a distinct, terminally differentiated population

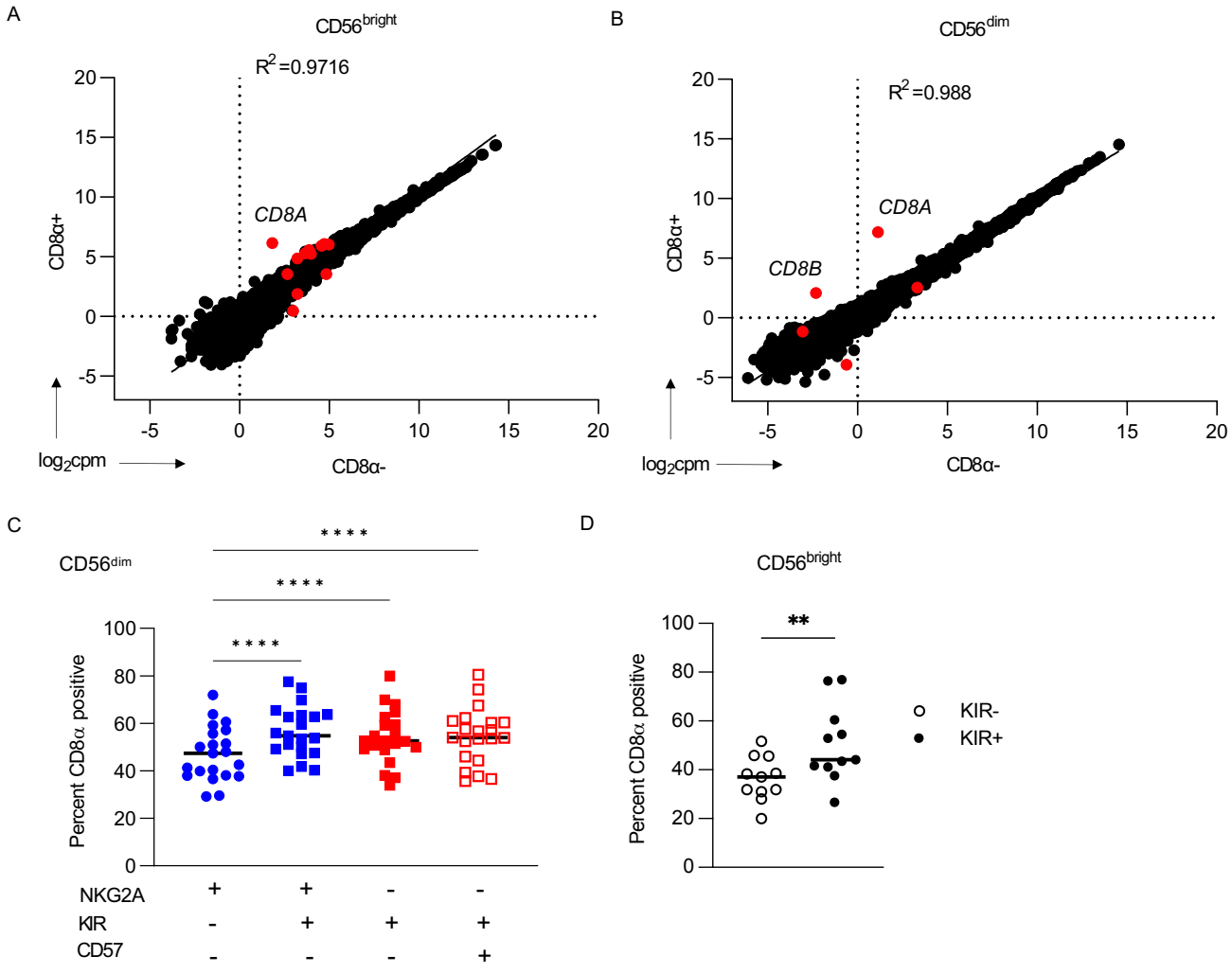

Figure 3: CD8α does not mark a distinct, terminally differentiated population. (A-B) Bulk RNA sequencing was performed on freshly isolated **(A)** CD56^{bright} or **(B)** CD56^{dim} NK cells sorted based on CD8α expression (CD3- CD19- CD14-). Data shown as the log_2 normalized expression of protein-coding genes in CD8α+/- populations. Red dots indicate genes that are statistically significantly differentially expressed (adjusted p-value <0.05). N= 6 unique donors. R^2 value derived from simple linear regression of gene expression data. **(C-D).** Peripheral blood NK cells were stained for expression of markers of NK maturation. **(C)** CD56^{dim} NK cell maturation stages were identified based on expression of NKG2A, KIR (KIR3DL1, KIR2DL1, and KIR2DL2/3), and CD57, with maturation increasing from left to right. Data shown as the percentage of each subset that is positive for CD8α expression. N=28 donors **(D)** Expression of CD8α within NKG2A- CD56^{bright} KIR- or KIR+ (KIR3DL1+, KIR2DL1+, and KIR2DL2/3+) NK cells. N=11 donors. Statistical significance was determined using (C) two-way ANOVA with

Holm-Šídák correction for multiple comparisons, and (D) two-tailed paired t-test. *p<0.05, **p<0.01, ***p<0.001, ****p<0.0001.

Figure 4: IL-15 modulates CD8α expression on CD8α- cNK cells

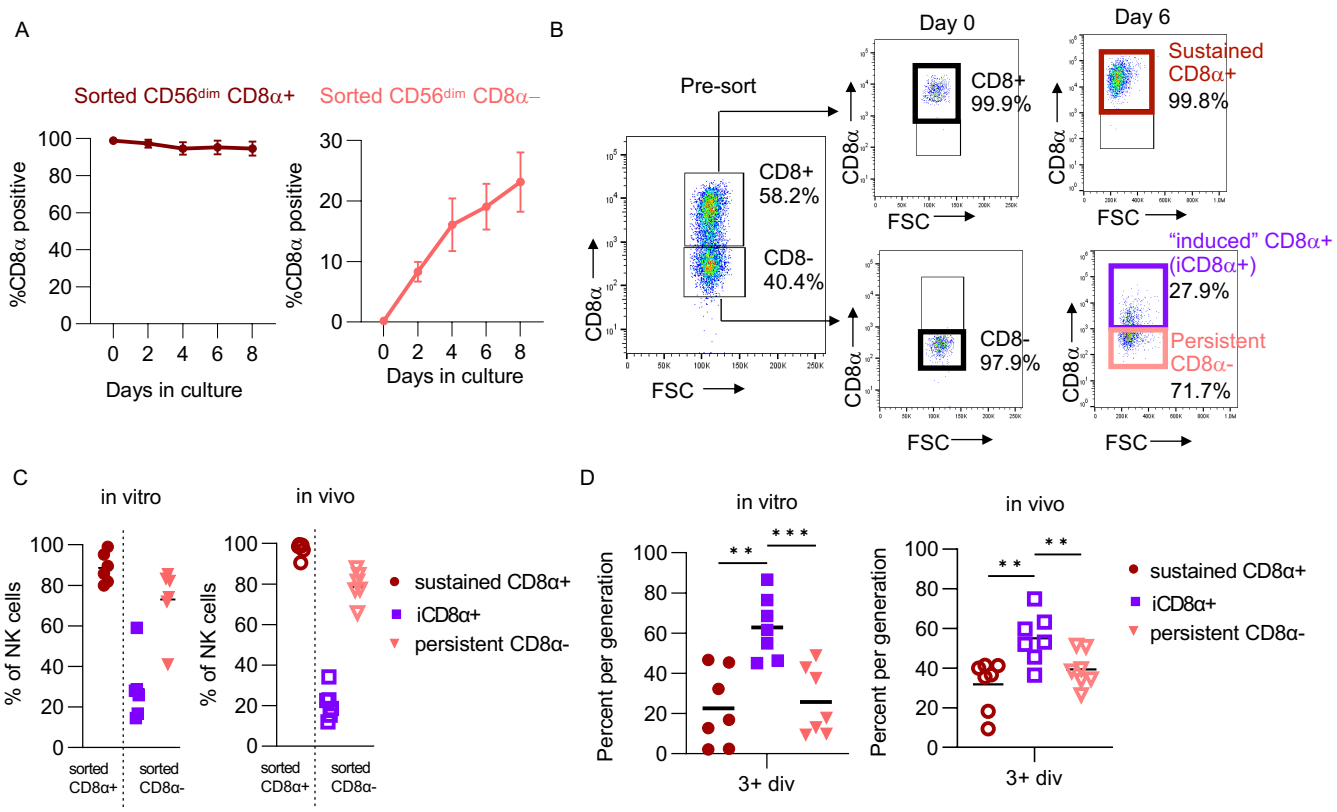

Figure 4: IL-15 modulates CD8α expression. (A) CD8α+/- CD56^{dim} NK cells were sorted and cultured in 5 ng/mL IL-15 for up to 8 days. Percentage of NK cells positive for CD8α expression, on cells originally sorted as CD8α+ or CD8α-. N=2-3 donors, 2 independent experiments. **(B)** Gating strategy for identification of 'induced' CD8α+ vs 'sustained' CD8α+ and 'persistent' CD8α- NK cells. Sorted CD8α+ NK cells that remained CD8α+ were defined as 'sustained' CD8α+. Sorted CD8α- NK cells that upregulated CD8α during culture were defined as 'induced' CD8α+". Sorted CD8α- NK cells that remained CD8α- during culture were defined as 'persistent' CD8α-" **(C-D)** CD8α+/- CD56^{dim} NK cells were sorted and cultured in 1 ng/mL IL-15 in vitro or into NSG mice supported with i.p. rh-IL-15 3x/week. Data shown as percent of NK cells positive for CD8α expression after 9 days. N= 8 donors, 4 independent experiments. **(D)** Percentage of NK cells undergoing 3 or more divisions within the indicated subsets in vitro or in vivo in NSG mice 9 days after sorting. N=6-9 donors and 4 independent experiments. Statistical significance was determined by two-way ANOVA with Holm-Šídák correction for multiple comparisons.

Figure 5: RUNX3 regulates CD8α expression

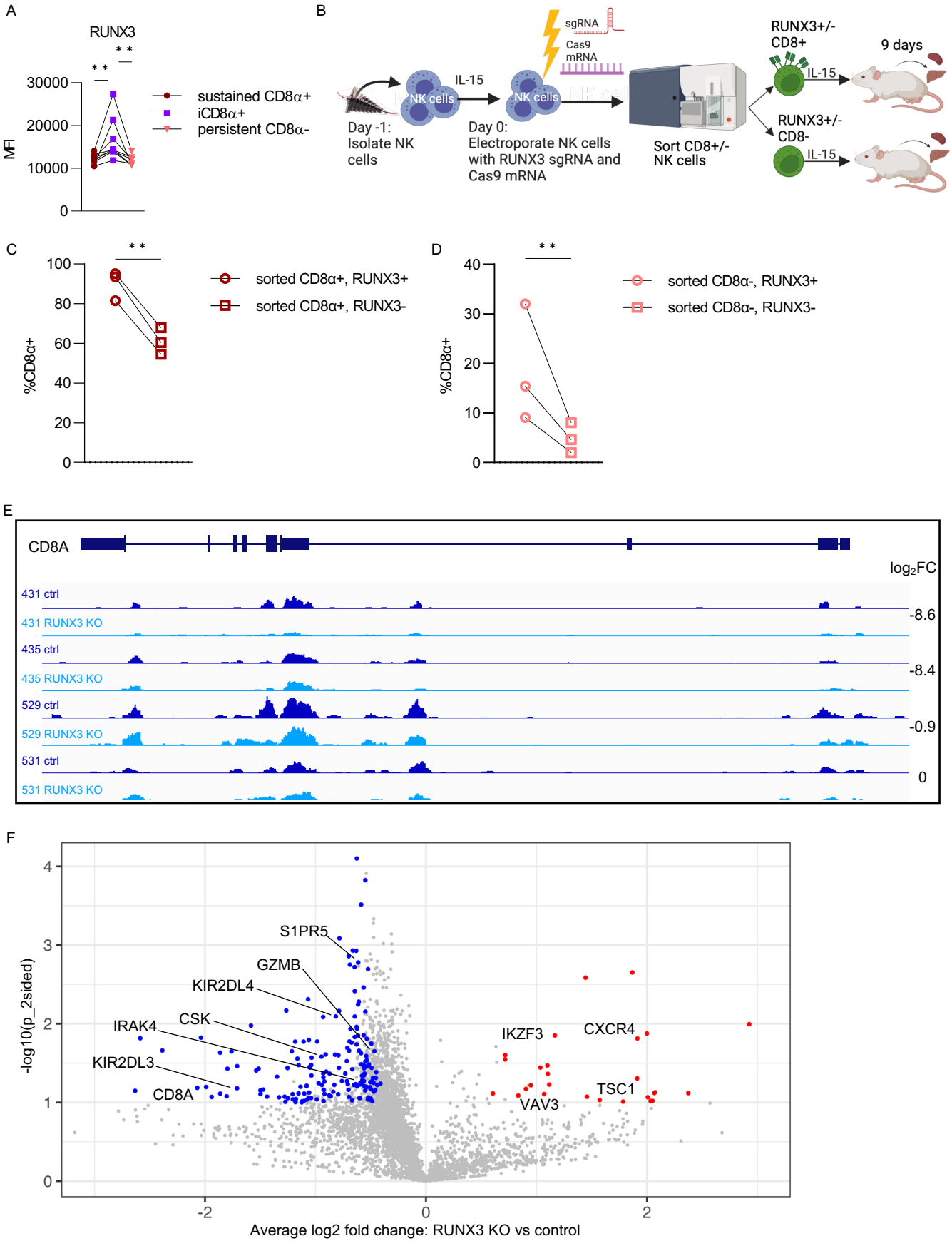

Figure 5: RUNX3 regulates CD8α expression. (A) MFI of RUNX3 on Day 6 within the indicated populations cultured in 1 ng/mL IL-15. N=5 donors, 3 independent experiments **(B-D)** NK cells were electroporated with RUNX3 sgRNA and Cas9 mRNA, cultured in vitro for 48 hours, then sorted based on CD8α expression. NSG mice were injected (I.V.) with sorted CD8α+/- control or RUNX3 KO cells, and supported with rh-IL-15 (I.P) for 9 days. **(B)** Experimental schema. **(C-D)** Percentage of human NK cells within the liver expressing CD8α within RUNX3+ or RUNX3- populations that were originally sorted as **(C)** CD8α+ or **(D)** CD8α-. Statistical significance was determined by (A) repeated measures one-way ANOVA, and (C-D) ratio paired two-tailed t-test. N=3 donors, 2 independent experiments. *p<0.05, **p<0.01. **(E-F)** NK cells were electroporated with control or RUNX3 gRNA and Cas9 mRNA, cultured in 5 ng/mL IL-15 for 9 days, and assessed for H3K27ac abundance using CUT&TAG. **(E)** IGV tracks showing H3K27ac peaks within the *CD8A* locus for control and RUNX3 KO donor pairs, with the log2FC for each donor pair for the entire CD8A locus shown. **(F)** Volcano plot showing the average log2 fold change and -log10 p of matched paired t-test for donor matched RUNX3 KO versus control H3K27ac signal for gene loci. Genes in red have significantly increased H3K27ac and genes in blue have significantly decreased H3K27ac in RUNX3 KO with log2FC cutoffs ≥absolute(0.5) for at least three of four donors. See Methods for determination of statistical significance. N=4 donors, 2 independent experiments.

Figure 6: iCD8α have greater IL-15R expression and signaling

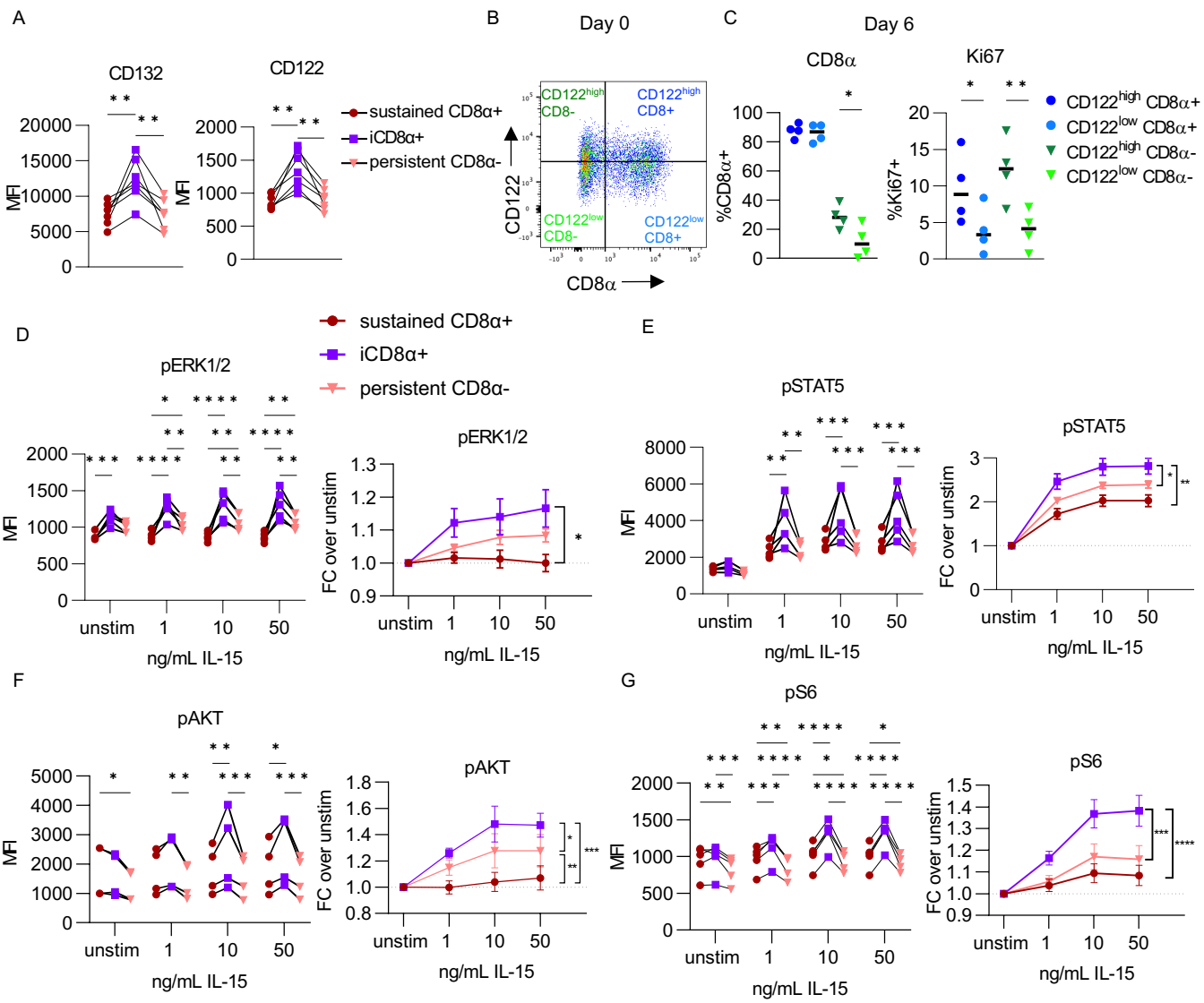

Figure 6: iCD8α have greater IL-15R expression and signaling. (A) Primary human NK cells were sorted into CD8α+ and CD8α- CD56^{dim} populations and cultured in vitro in 1 ng/mL IL-15 for 6 days. CD132 and CD122 expression was assessed by flow cytometry, gated within the indicated subsets. N=7 donors, 3 independent experiments. **(B-C)** CD56^{dim} NK cells were sorted from freshly isolated primary human NK cells, based on high and low expression of CD122 and CD8α, and cultured for 6 days in vitro in 5 ng/mL IL-15. **(B)** Representative flow plots of gating strategy for cell sorting. **(C)** Summary data showing the percentage of NK cells positive for CD8α or Ki67 expression that were originally sorted as CD122^{high} or CD122^{low}, CD8α+ or CD8α-. N=4 donors, 2 independent experiments. **(D-G)** CD8α+ and CD8α- CD56^{dim} NK cells were sorted and cultured for 6 days in vitro with 1 ng/mL IL-15. Cells were cultured briefly (1 hr) in cytokine-free media prior to stimulation with the

indicated concentrations of IL-15 for 1 hour. Data shown as the MFI and fold change over the unstimulated condition within the indicated subsets for **(D)** pERK1/2, **(E)**, pSTAT5, **(F)** pAKT, and **(G)** pS6. n=5 donors, 2 independent experiments. Statistical significance was determined using (A and C) RM one-way ANOVA, and (D-G) two-way ANOVA with Holm-Šídák correction for multiple comparisons. *p<0.05, **p<0.01, ***p<0.001, ****p<0.0001.

Figure 7: Induced CD8α expression is associated with metabolic activity in NK cells

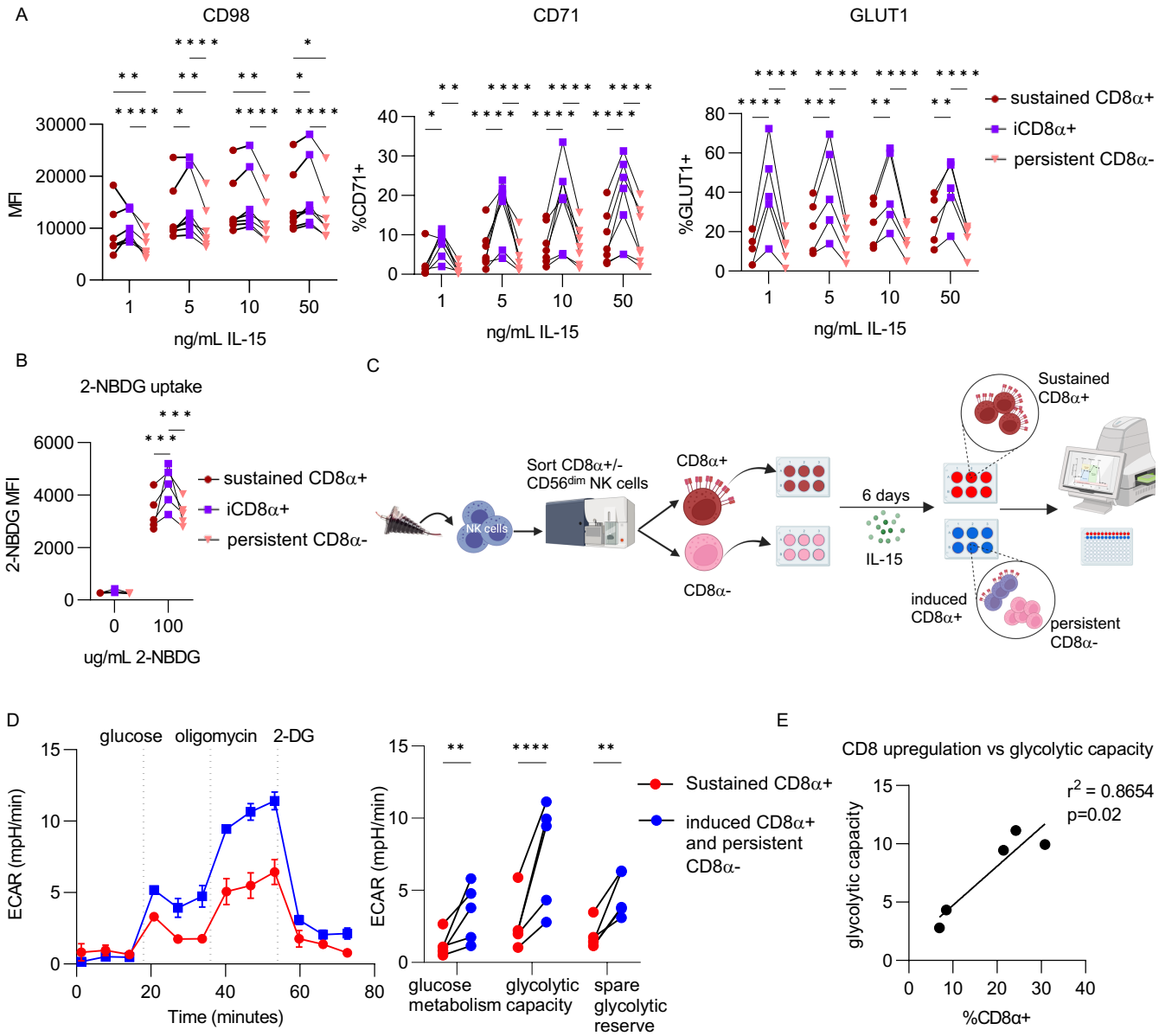

Figure 7: Induced CD8α expression is associated with metabolic activity in NK cells. **(A)** Primary human NK cells were sorted into CD8α+ and CD8α- CD56^{dim} populations and cultured for 6 days in vitro with the indicated concentrations of IL-15. MFI or percentage of NK cells positive for nutrient receptors CD98, CD71, and GLUT1 are shown. N=7 donors, 3 independent experiments. **(B-E)** CD8α+ and CD8α- NK cells were sorted and cultured for 6 days in vitro 1 ng/mL IL-15. **(B)** Uptake of the fluorescent glucose analog 2-NBDG at various concentrations was assessed by flow cytometry. The MFI of 2-NBDG within the indicated subsets is shown. N= 7 donors, 3 independent experiments. **(C-E)** Metabolic parameters were using the Seahorse XFe96 Extracellular

Flux Analyzer. **(C)** Experimental schema. **(D)** Donor glycolysis stress test trace from one representative donor, with measurement of extracellular acidification rate (ECAR) with the indicated stimulation and summary data showing glucose metabolism, glycolytic capacity, and glycolytic reserve. (**E)** Simple linear regression showing the relationship between the extent of CD8α upregulation within the sorted CD8α- CD56^{dim} NK cells and the glycolytic capacity recorded via Seahorse. N=6 donors from 4 independent experiments. Statistical significance was determined using two-way ANOVA with Holm-Šídák correction for multiple comparisons. *p<0.05, **p<0.01, ***p<0.001, ****p<0.0001.

Figure 8: Induction of CD8α corresponds to enhanced in vitro and ex vivo responses to tumors

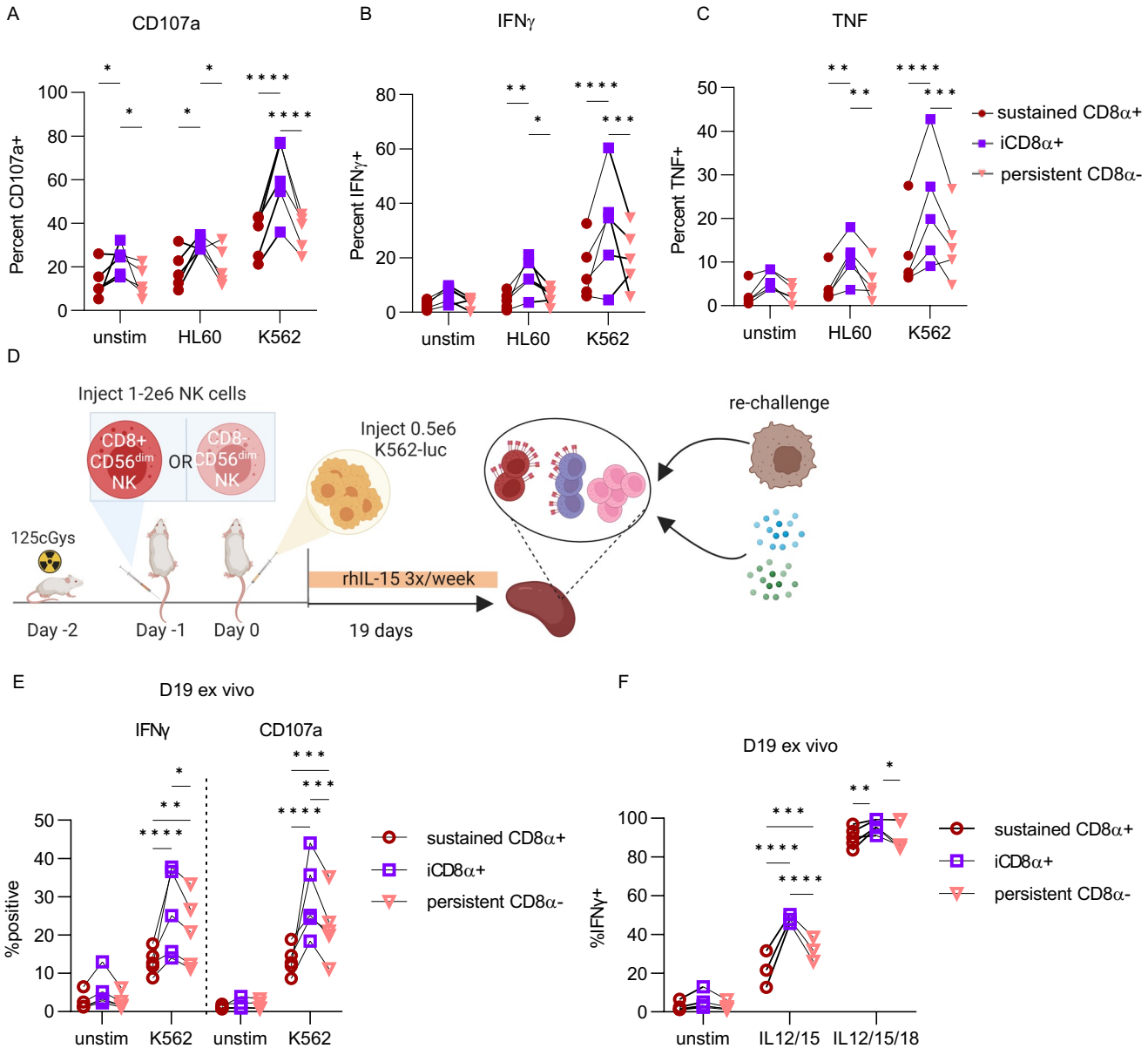

Figure 8: Induction of CD8α corresponds to enhanced in vitro and ex vivo responses to tumors. (A-C) Primary human NK cells were sorted into CD8α+ and CD8α- CD56^{dim} populations and cultured in vitro in 5 ng/mL IL-15 for 6 days. NK cells were stimulated with HL60 or K562 leukemic cell lines at a 1:1 Effector:Target ratio for 6 hours, with GolgiPlug/Stop for the last 5 hours. Data shown as the percentage of NK cells expressing **(A)** CD107a, **(B)** IFNγ, or **(C)** TNF, within the indicated subsets. N=5 donors, 3 independent experiments **(D-F)** CD56^{dim} NK cells were sorted based on CD8α expression, and approximately 1x10^6 to 2x10^6 CD8α+ or CD8α - CD56^{dim} NK cells were injected intravenously (tail-vein) into NSG mice (D-1). The next day, 0.4-0.5x10^6 K562-

CBR cells were injected i.v. (tail-vein) (D0). NK cells were supported with i.p. rh-IL-15 3x/week. **(D)** Experimental schema. **(E-F)** On Day 19, splenocytes were isolated from NK cell-treated mice and stimulated ex-vivo with **(E)** K562s (10:1 splenocyte to K562 ratio) or **(F)** cytokines for 6 hours (IL-12 20 ng/mL, IL-15 100 ng/mL, IL-18 100 ng/mL) with GolgiPlug/Stop in the last 5 hours. The percentage of NK cells positive for the indicated marker and gated within the indicated subsets is shown. N=5 donors, 3 independent experiments. Statistical significance determined by two-way ANOVA with Holm-Šídák correction for multiple comparisons. *p<0.05, **p<0.01, ***p<0.001, ****p<0.0001.

Figure 9: : CD8 KO enhances cytokine secretion and degranulation following NKp30 stimulation

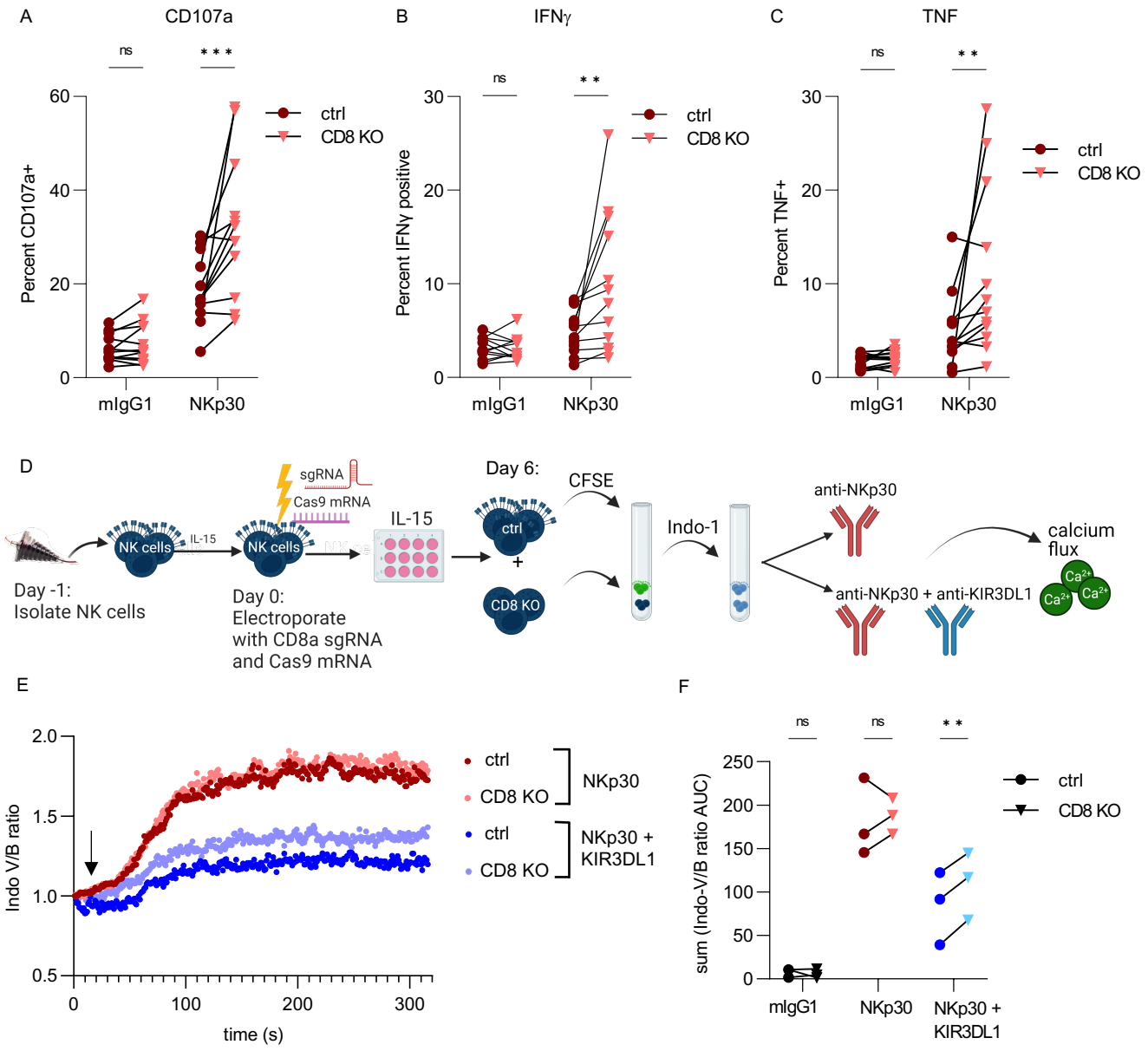

Figure 9: CD8A knockout enhances cytokine secretion and degranulation following NKp30 stimulation. **(A-C)** Primary human NK cells were electroporated with Cas9 mRNA and sgRNA targeting *CD8A* or a control gRNA (*TRAC*) and cultured in vitro in 1 ng/mL IL-15 for 6 days. NK cells were stimulated by plate-bound antibodies (10 µg/mL) targeting NKp30 or mouse IgG1 isotype control antibody for 6 hours, with GolgiPlug/Stop in the last 5 hours. Percentage of NK cells positive for expression of **(A)** CD107a, **(B)** IFNγ, or **(C)** TNF is shown. N=13 donors, 7 independent experiments. **(D-F)** Control or CD8A KO cells were labeled with 50 nM CFSE, mixed together at a 1:1 ratio, then labeled with the UV-excitable Ca^{2+}-sensing dye Indo-1. Monoclonal antibody (5

μg/mL) targeting NKp30 alone, or NKp30 (5 μg/mL) and KIR3DL1 (0.2 μg/mL) was added for 20 min at 4°C, cells were washed, then cross-linking was induced at the indicated time point (black arrow) using goat anti-mouse IgG (10 μg/mL). Calcium flux was measured by flow cytometry. **(E)** Data shown as the normalized ratio of indo-violet over indo-blue within control or CD8A KO cells as a function of time, in one representative donor. **(F)** Sum of the area under the curve (AUC) of the normalized indo-violet / indo-blue ratio for all time points in control or CD8 KO cells. N=3 donors, 3 independent experiments; donors were pre-screened to ensure KIR3DL1 and CD8α expression of >30%. Statistical significance was determined by (A-C) two-way ANOVA with Holm-Šídák correction for multiple comparisons and (F-G) two-tailed paired. t-test ns = not significant *p<0.05, **p<0.01, ***p<0.001, ***p<0.0001.